Computers and Geotechnics 125 (2020) 103660

Contents lists available at ScienceDirect

Computers and Geotechnics

journal homepage: www.elsevier.com/locate/compgeo

Research Paper

Novel Bayesian framework for calibration of spatially distributed physical-based landslide prediction models.

Ivan Depina[a,b,*], Emir Ahmet Oguz[c], Vikas Thakur[c]

[a] SINTEF, Department of Rock and Geotechnical Engineering, Trondheim, Norway
[b] University of Split, Faculty of Civil Engineering, Architecture and Geodesy, Split, Croatia
[c] Norwegian University of Science and Technology, Department of Civil and Environmental Engineering, Trondheim, Norway

ARTICLE INFO

Keywords:
Landslide
Rainfall
Physical-based
Calibration
Statistics
Bayes
Hazard

ABSTRACT

This study presents a novel Bayesian framework for statistical calibration of spatially distributed physical-based landslide prediction models. The calibration process is formulated in a statistical setting with the model parameters simulated as spatially variable with random fields and the model calibration defined within the Bayesian framework. The implementation of such calibration process is challenging due to large numbers of calibration parameters and high-dimensional likelihood functions, which are central in establishing a relation between observations and the corresponding model predictions. The former challenge was resolved by reformulating the Bayesian updating problem as an equivalent reliability problem and solving it with efficient reliability methods. The latter challenge was resolved by developing novel lower-dimensional approximate likelihood formulations, suitable for the interpretation of landslide initiation zones, based on the Approximate Bayesian Computation method. The novelties of the proposed approach stem from describing landslide model parameters as spatially variable, development of a statistical framework to calibrate landslide prediction models, and introduction of approximate likelihood formulations.

1. Introduction

Landslides are a major threat to the global population, resulting in substantial annual losses of life and damage to property throughout the world (e.g., Petley, 2012). They are commonly characterized by the movement of a mass composed of soil, rock, debris, and artificial fills down a slope, under the influence of gravity (e.g., Varnes, 1958). Landslides are triggered by different phenomena including precipitation, snowmelt, rapid temperature changes, earthquakes, and human activities. Recent climate trends indicate an increase in temperature and precipitation in some areas of the world, which may increase the frequency of landslide triggering events such as extreme rainfall, snowmelt and temperature changes (e.g., Gariano and Guzzetti, 2016). Combined with growing population and expanding land usage, societal risk associated with rainfall-induced landslides are likely to increase over time.

Increasing rainfall-induced landslide risks necessitate the development and implementation of efficient landslide risk management strategies (e.g., Dai et al., 2002). Among the various strategies, Monitoring and Early Warning (MEW) systems are often deployed as a cost-efficient landslide risk management strategy (e.g., Pecoraro et al., 2018). One of the central elements of an MEW-based strategy is the capacity to support risk reduction with improved rainfall-induced landslide hazard assessment and reductions of consequences. Such capacity is enabled by an efficient integration of various data sources (e.g., monitoring data, landslide inventories) into rainfall-induced landslide prediction models. Rainfall-induced landslide prediction models can be classified with respect to the underlying formulation into statistical- and physical-based models.

The focus of this study is on the calibration of physical-based models, which rely on the solutions of coupled hydro-mechanical differential equations to capture the effects of rainfall infiltration and groundwater flow on slope stability in unsaturated soils. Several physical-based models have been successfully applied to rainfall-induced landslide assessment including Transient Rainfall Infiltration and Grid-Based Regional Slope-Stability (TRIGRS) (Baum et al., 2002), Shallow Landslides Instability Prediction (SLIP) (Montrasio and Valentino, 2008), GEOtop-FS (Simoni et al., 2008), Stability Index Mapping (SINMAP) (Pack et al., 1998), r.rotstab (Mergili et al., 2014), and Shallow Slope Stability models (SHALSTAB) (Montgomery and Dietrich, 1994). Comparison of some of these models in Zizioli et al. (2013) and Schilirò et al. (2016) reveals that the models often achieve

* Corresponding author.
E-mail address: ivan.depina@sintef.no (I. Depina).

https://doi.org/10.1016/j.compgeo.2020.103660
Received 8 February 2020; Received in revised form 29 April 2020; Accepted 14 May 2020
Available online 08 June 2020

similar levels of accuracy in predicting shallow landslides. This study will examine the performance of the TRIGRS model to simulate the timing and spatial distribution of shallow, rainfall-induced landslides (Baum et al., 2002). More detailed examination of the TRIGRS features is presented in the following sections.

One of the central elements in the implementation of TRIGRS and other physical-based model is model calibration due to paucity of input data on time-varying rainfall, topographic, soil thickness, initial water table depth, material strength, and hydraulic properties (Salciarini et al., 2006). Several additional studies demonstrated the importance of calibration with the use of probabilistic approaches (e.g., Canli et al., 2018; Melchiorre and Frattini, 2012; Khalaj et al., 2020; Zhang et al., 2009; Zhang et al., 2010) to account for the effects of parameter uncertainty in model calibration, sensitivity analysis and landslide predictions. Although the effects of parameter variability were taken into account in earlier studies, modeling spatial variability of input parameters within a single geological formation is an existing challenge (Zieher et al., 2017). This study aims to investigate the effects of spatial variability on calibration and predictions of physical-based prediction models (i.e., TRIGRS). Spatial variability of model parameters will be explicitly modeled by random fields, being variable in the horizontal directions and constant in the vertical direction. Explicit modeling of spatial variability is considered advantageous as it enables advanced calibration and fine-tuning of the model to account for the inherent spatial variability in soil properties and local variations in physical, geological and hydrological conditions.

Explicit modeling of spatial variability has been mainly reserved for single-slope models (e.g., Cai et al., 2017; Santoso et al., 2011; Fenton and Griffiths, 2008; Liu et al., 2018) with some studies on spatially-distributed landslide models (e.g., Wang et al., 2019; Chen and Zhang, 2014). For example, the effects of spatial variability in soil cohesion, friction angle and hydraulic conductivity along the vertical direction on the stability of a single slope were examined in Cai et al. (2017). Kriging model was implemented in Chen and Zhang (2014) to interpolate spatially varying rainfall distribution and provide inputs to predict regional rainfall-induced slope failures in layered soils. Simulations of spatially variable soil strength parameters in the vertical and the along-slope direction were conducted in Fenton and Griffiths (2008) to examine its effects on the propagation of slope failure and slope reliability. Additionally, Bayesian networks were used in Wang et al. (2019) to update landslide susceptibility and distributions of spatially variable properties based on monitoring data.

Given the importance of model calibration to the implementation of physical-based landslide prediction models, it is necessary to develop efficient strategies for integration of information from various data sources into the spatially variable models of uncertain model parameters. Building on the statistical framework of spatially variable properties, the model calibration will be defined in the setting of Bayesian updating. Bayesian updating is selected as it provides an explicit and consistent approach to calibrate the distribution of spatially variable parameters with information from various data sources (e.g., Straub, 2011; Straub and Papaioannou, 2014; Khalaj et al., 2020; Papaioannou and Straub, 2012; Yang et al., 2018). However, implementation of spatial variability introduces several challenges in the calibration process of a physical-based landslide model including high-dimensional parameters spaces and high-dimensional likelihood functions. The former challenge is resolved by adopting the Bayesian updating with Structural reliability methods (BUS) (Straub and Papaioannou, 2014), which is well suited for solving high-dimensional Bayesian updating problems. Resolving the latter challenge is of high importance as the likelihood function is central in the implementation of the Bayesian updating because it relates the observations (e.g., measurements, slope failure) to model predictions thus enabling updating of model parameters. This challenge arises in updating problems with relatively large number of observations, resulting in high-dimensional likelihood functions. Evaluating such likelihood functions is challenging because their values can become very low and computationally intractable. This challenge is resolved by developing approximate likelihood formulations. The developments are based on the Approximate Bayesian Computation (ABC) method (e.g., Sisson et al., 2018), where a lower-dimensional likelihood function is formulated based on certain summary statistics to avoid computational difficulties of the higher-dimensional full likelihoods. Different types of approximate likelihood formulations specific for physical-based landslide prediction models are proposed and discussed to evaluate their effects on the updating process. The novelties of this study stem from describing landslide model parameters as spatially variable, development of a statistical framework to calibrate landslide prediction models, and introduction of approximate likelihood formulations.

2. A short description of the TRIGRS model

TRIGRS supports rainfall infiltration models that simulate the development of groundwater pressures for tension-saturated and unsaturated initial conditions (Baum et al., 2002). The rainfall infiltration model for tension-saturated initial conditions is based on the linearized solution of the Richards equation (Iverson, 2000) and its extensions (Baum et al., 2002). The solution consists of a steady, $\psi_0(z)$, and a transient, $\psi_t(z, t)$, groundwater pressure head components:

$$\psi(z, t) = \psi_0(z) + \psi_t(z, t) \tag{1}$$

where z is the depth from the ground surface in the vertical direction, and t is time. The steady-state component depends on the initial position of the depth of the water table from the ground surface, d, steady surface flux, I_{Z0}, slope angle, δ, and the saturated conductivity in the vertical direction, k_S, (e.g., Baum et al., 2002; Iverson, 2000):

$$\psi_0(z) = (z - d)[\cos^2\delta - I_{Z0}/k_S] \tag{2}$$

The prediction of $\psi_t(z, t)$ for tension saturated initial conditions assumes a one-dimensional, vertical downward flow with a time-varying flux at the ground surface and a zero flux at an impermeable basal boundary at a finite depth (Baum et al., 2002), with the formulation provided in Appendix A due to a lengthy expression. Runoff routing algorithm is implemented in TRIGRS to route the surface runoff from areas with excess surface water to adjacent downslope areas that can absorb it or route it further down (Baum et al., 2002). The estimate of the transient groundwater pressure head, $\psi(z, t)$, is then provided to the slope stability model. The stability of a slope is evaluated based on the factor of safety, F_S, as a ratio of resisting friction forces over driving gravitational forces:

$$F_S\left(\boldsymbol{x}, z, t\right) = \frac{\tan\phi}{\tan\delta} + \frac{c - \psi(z, t)\gamma_w\tan\phi}{\gamma_s z\sin\delta\cos\delta} \tag{3}$$

where $\boldsymbol{x} = [c, \phi, \delta, G_s, e, \gamma_w, k_S, D_0, \theta_s, \theta_r]^T$ is a vector of model parameters, c is the effective stress cohesion, ϕ is the effective stress soil friction angle, γ_w is the water unit weight, $\gamma_s = (G_s + e)\gamma_w/(1 + e)$ is the average soil unit weight along depth with G_s being the specific gravity of the soil and e is the void ratio, θ_s and θ_r are, respectively, the saturated and residual volumetric water contents. In the unsaturated soil zone, the matric suction $\psi(z, t)\gamma_w$ is multiplied with the Bishop's effective stress parameter $\chi = (\theta - \theta_r)/(\theta_s - \theta_r)$ as an approximation of the suction-stress characteristic curve (Baum et al., 2002). Slope stability assessment will be conducted by evaluating the minimum factor of safety along depth as follows:

$$F_S\left(\boldsymbol{x}, t\right) = \min_{z\in[0,H]} F_S\left(\boldsymbol{x}, z, t\right) \tag{4}$$

where H is the depth to bedrock. A slope is considered as stable at time t if $F_S(\boldsymbol{x}, t) > 1$ and unstable otherwise.

The implemented rainfall infiltration, runoff routing and slope stability models are associated with several assumptions and

simplifications that introduce limitations to the applicability of the TRIGRS model. Some of these include (Baum et al., 2002) the assumption of a homogeneous, isotropic soil within a single cell, one-dimensional vertical infiltration that may not be the dominant flow process during longer storms and between storms, high sensitivity to the initial groundwater conditions, simple runoff routing algorithm not accounting for evapotranspiration and stream flow, simple infinite slope stability model, and inability to account for the post failure conditions (e.g., Calvello et al., 2017).

3. Statistical framework

3.1. Spatially variable soil properties

Soils are heterogeneous materials formed by diverse geological processes including changes in stresses, pore fluids, physical and chemical properties. Therefore, it is common to observe variations of physical properties of soils across different locations within a single deposit. Spatial variability of soil properties is often modeled with a continuous random field model. Random field is a statistical model that takes into account the point variability and the spatial dependence of soil properties. The point variability characterizes the uncertainties in soil properties at a location within the deposit with a probability density function (pdf). Spatial dependence is a property of natural soil deposits, where the similarity or dependence between soil properties at two locations in a deposit decays as the separation distance between the locations increases.

Spatial variability of soil properties is modeled in this study by adopting the Gaussian and lognormal random field models. Two-dimensional Gaussian and lognormal random field models are implemented to model the spatial variability of soil properties in the horizontal directions. Spatial variability in the vertical direction is not modeled due to lack of capacity in TRIGRS to integrate such effects in the implemented formulations.

Only the Gaussian random field model will be presented here because a lognormal random field can be easily transformed to a Gaussian random field. Consider a set of spatial instances, $l_1, \ldots, l_{n_r}$, representing locations in a two-dimensional domain. A Gaussian random field of a soil property, $K(l)$, defines the joint pdf of $K(l_1), \ldots, K(l_{n_r})$ as a multivariate normal pdf:

$$f_{\mathbf{K}}(\kappa) = \frac{1}{(2\pi)^{n/2}|\boldsymbol{C}|^{1/2}} \exp\left[-\frac{1}{2}(\kappa-\mu)^T \boldsymbol{C}^{-1}\left(\kappa-\mu\right)\right] \tag{5}$$

where the mean vector is specified by the mean values of the random field, $\mu = [\mu(l_1), \ldots, \mu(l_{n_r})]^T$, while the elements of the covariance matrix, $\boldsymbol{C}$, are defined as follows:

$$C_{ij} = \begin{cases} C(l_i, l_j) = \sigma^2(l_i) & \text{if } i = j \\ C(l_i, l_j) = \sigma(l_i)\sigma(l_j)\rho(l_i, l_j) & \text{if } i \neq j \end{cases} \tag{6}$$

where $\rho(l_i, l_j); i, j = 1, \ldots, n_r$ is the correlation coefficient defined by an autocorrelation function. The elliptical autocorrelation function is adopted:

$$\rho\left(l_i, l_j\right) = \exp\left\{-2\sqrt{\left(\frac{\tau_x}{l_x}\right)^2 + \left(\frac{\tau_y}{l_y}\right)^2}\right\} \tag{7}$$

where $\tau_x = |x_i - x_j|$ and $\tau_y = |y_i - y_j|$ are distances between l_i and l_j, and l_x and l_y are correlation lengths along the x and y directions, respectively.

3.2. Bayesian updating

The availability of additional sources of information (e.g., monitoring, landslide inventories, remote sensing) supports a learning process in which uncertainties in spatially variable soil properties can be reduced. Reducing uncertainties enables advanced calibration and fine-tuning of the model to local variations in geotechnical and hydrological parameters for more reliable and consistent landslide predictions. One of the approaches for integrating information with existing models is Bayesian updating. In Bayesian updating, a prior probabilistic landslide prediction model is updated with additional information to obtain a posterior probabilistic model. The Bayesian framework allows for integration of uncertain and incomplete information and quantification of accuracy in the posterior model (e.g., Straub and Papaioannou, 2014). The implementation of Bayesian updating in this study is based on the Bayesian updating with structural reliability methods (BUS) algorithm (Straub and Papaioannou, 2014).

To further investigate the Bayesian framework, consider a landslide prediction model with a vector of uncertain model parameters, $\boldsymbol{X} = [X_1, \ldots, X_n]^T$(e.g., geotechnical and hydrological parameters). The joint distribution of these parameters is denoted as $f'(\boldsymbol{x})$. With the provision of additional information on the model parameters (e.g., field investigations) or the model performance (e.g., deformation measurements, slope failure), the prior joint pdf, $f'(\boldsymbol{x})$, can be updated to a posterior joint pdf, $f''(\boldsymbol{x})$ through the Bayesian framework as follows:

$$f''(\boldsymbol{x}) = \frac{L(\boldsymbol{x})f'(\boldsymbol{x})}{\int_X L(\boldsymbol{x})f'(\boldsymbol{x})d\boldsymbol{x}} \propto L(\boldsymbol{x})f'(\boldsymbol{x}) \tag{8}$$

where $\boldsymbol{x}$ is a realization of the uncertain model parameters, $L(\boldsymbol{x})$ is the likelihood function. Evaluation of the denominator or the normalizing constant is usually omitted from implementations of Bayesian updating. $L(\boldsymbol{x})$ is central in the implementation of the Bayesian framework as it relates observations to the values of the uncertain parameters:

$$L(\boldsymbol{x}) \propto \Pr(\text{Observation}|\boldsymbol{X} = \boldsymbol{x}) \tag{9}$$

One of the approaches for specifying $L(\boldsymbol{x})$ is to relate the observations to the uncertain parameters by considering them as model outcomes (e.g., Straub and Papaioannou, 2014). Let us consider an observation, y_i(e.g., pore pressure measurement, failed slope) and the corresponding model prediction, $h_i(\boldsymbol{x})$. $h_i(\boldsymbol{x})$ is associated with a model prediction error ϵ_i, distributed according to the pdf f_{ϵ_i}:

$$y_i = h_i(\boldsymbol{x}) + \epsilon_i \tag{10}$$

$L(\boldsymbol{x})$ can be specified to account for equality and inequality types of information (e.g., Straub, 2011; Straub and Papaioannou, 2014). An example of equality types of information might be pore pressure or deformation measurements in a slope, while inequality information might include the observation of a stable slope or bearing capacity of a geotechnical system exceeding working loads. In the case of an equality information, $L(\boldsymbol{x})$ is calculated as follows:

$$L_i(\boldsymbol{x}) = f_{\epsilon_i}\left[y_i - h_i(\boldsymbol{x})\right]$$

Assuming a normal model error, $\epsilon_i \sim N(\mu_{\epsilon_i}, \sigma_{\epsilon_i})$, $L(\boldsymbol{x})$ can be defined as follows:

$$\begin{aligned} L_i(\boldsymbol{x}) &= \Pr(y_i - h_i(\boldsymbol{x}) = \epsilon_i|\boldsymbol{X} = \boldsymbol{x}) \\ &= \Pr\left(\frac{y_i - h_i(\boldsymbol{x}) - \mu_{\epsilon_i}}{\sigma_{\epsilon_i}} = \frac{\epsilon_i - \mu_{\epsilon_i}}{\sigma_{\epsilon_i}}\middle|\boldsymbol{X} = \boldsymbol{x}\right) \\ &= \Pr\left(\frac{y_i - h_i(\boldsymbol{x}) - \mu_{\epsilon_i}}{\sigma_{\epsilon_i}} = U\middle|\boldsymbol{X} = \boldsymbol{x}\right) \\ &= \phi\left(\frac{y_i - h_i(\boldsymbol{x}) - \mu_{\epsilon_i}}{\sigma_{\epsilon_i}}\middle|\boldsymbol{X} = \boldsymbol{x}\right) \end{aligned} \tag{11}$$

where $U \sim N(0, 1)$ is a standard normal random variable with the probability and the cumulative density functions denoted, respectively, as ϕ and Φ.

$L(\boldsymbol{x})$ for the inequality type of information can be expressed as an observation event Z_i:

$$Z_i = \{\boldsymbol{x} \in \mathbb{R}^n : y_i - h_i(\boldsymbol{x}) \leqslant \epsilon_i\} \tag{12}$$

where $\mathbb{R}^n$ is n-dimensional real space. Assuming a normal model error, $\epsilon_i \sim N(\mu_{\epsilon_i}, \sigma_{\epsilon_i})$, $L(\boldsymbol{x})$ can be defined as follows:

$$L_i(\boldsymbol{x}) = \Pr(Z_i|\boldsymbol{X}=\boldsymbol{x}) = \Pr(y_i - h_i(\boldsymbol{x}) \leqslant \epsilon_i|\boldsymbol{X}=\boldsymbol{x}) = 1 - \Phi\left(\frac{y_i - h_i(\boldsymbol{x}) - \mu_{\epsilon_i}}{\sigma_{\epsilon_i}}\middle|\boldsymbol{X}=\boldsymbol{x}\right) \quad (13)$$

In the case of m statistically independent observations, the combined likelihood of all of the observations is defined as:

$$L(\boldsymbol{x}) = \prod_{i=1}^{m} L_i(\boldsymbol{x}) \quad (14)$$

Conversely, for dependent observations the likelihood function is specified as a joint pdf of all ϵ_i (Straub and Papaioannou, 2014). The implementation of Bayesian updating in this study is based on Bayesian Updating with Structural Reliability Methods (BUS) algorithm, where the updating problem is expressed as a reliability problem with more details provided in Straub and Papaioannou (2014).

4. Bayesian updating of a physical-based landslide prediction model

The application of Bayesian updating to a physical-based landslide prediction model with spatially variable properties can be challenging due to high-dimensionality of the updating problem and difficulties with evaluating the likelihood function. Strategies for addressing these challenges will be discussed in the following sections.

4.1. Dimensionality of the updating problem

Challenges with high-dimensional updating problems are likely to occur in situations when the landslide prediction model parameters are considered as spatially variable. Explicit modeling of spatially variable model parameters with random fields can be done by adapting the random field discretization to the grid of a physical-based landslide prediction model. The grid of landslide prediction models often contains hundreds or thousands of cells as the applications of physical-based landslide prediction models commonly involve large areas. A random field with the discretization adapted to the discretization of the landslide prediction model would therefore likely result with a large set of random variables. A large set of random variables can lead to potential difficulties in the implementation of the BUS method, as the Bayesian updating problem is reformulated as a reliability problem. A reliability problem is defined as solution to a multidimensional integral, with the dimensionality of the integral in the BUS method being $n + 1$, where n is the number of random variables and the additional random variable is the standard uniform variable augmenting the set of random variables in the BUS method. The challenge of solving a high-dimensional reliability integral can be mitigated by implementing a reliability method that is not affected by the dimensionality of the problem (e.g., Au and Beck, 2001; Schuëller et al., 2004). Therefore, the Subset Simulation (SUS) method (Au and Beck, 2001) has been implemented in this study due to its efficiency and stable performance in high-dimensional reliability problems (Schuëller et al., 2004).

4.2. Likelihood formulations

The application of Bayesian updating to physical-based landslide prediction models can be also challenging due to difficulties with formulating and evaluating the likelihood function. Several formulations of the likelihood function specific to updating parameters of a physical-based landslide prediction model on historical landslide events will be discussed in the following section. Historical landslide events often include limited information on the triggering conditions of a landslide such as categorical data on slope failing or being intact (i.e., slope survival) after a given rainfall event with the corresponding locations of slope failures. Such information present indirect observations of the model parameters because the stability of a slope depends on intricate interactions between the various topographical, geotechnical, hydrological and meteorological landslide triggering parameters. One of the approaches for establishing a relationship between the indirect observations and the landslide triggering parameters is to implement a statistical or a physical-based landslide prediction model that can simulate slope response for varying combinations of the triggering parameters. This study focuses on physical-based models, which are often implemented as a black-box forward model, taking triggering parameters as input and simulating output in terms of a measure of slope stability (e.g., factor of safety).

The formulation of the likelihood function can significantly depend on the interpretation of the relation between the observation and the model predictions. It is important to note that the information on slope failure or survival is relevant only for the elements of the landsliding process that are captured by the physical-based model. In the case of TRIGRS, only information on the initiation zone of a landslide can be related to the model predictions, while the run-out zone and post-failure behavior are not simulated by the model. Furthermore, the interpretation of the information on the initiation of landslides can lead to several formulations of the likelihood function.

4.2.1. Marginal likelihood formulation

One of the approaches for formulating the likelihood function is to specify the likelihood function independently for each of the grid cells of the physical-based model. An illustration of the landslide initiation zone and the corresponding discretization onto the grid cells of the landslide prediction model is presented in Fig. 1.

For the cells where landslide initiation has been observed, this observation event can be expressed with the factor of safety greater than one at the start of the rainfall event, $F_S(\boldsymbol{x}, t=0) > 1$, and the factor of safety equal to or lower than one after the rainfall event, $F_S(\boldsymbol{x}, t=T) \leqslant 1$, where T is the duration of the rainfall event. The corresponding observation event is defined as follows:

$$Z_F = \{\boldsymbol{x} \in \mathbb{R}^n : \max[1 - F_S(\boldsymbol{x}, t=0), \min_{t\in(0,T]} F_S(\boldsymbol{x}, t) - 1] \leqslant \epsilon\} \quad (15)$$

Note that the observation is satisfied with negative values of the function specifying the observation event. Assuming the same normal model error for all the cells in the model, $\epsilon \sim N(\mu_\epsilon, \sigma_\epsilon)$, the likelihood function can be specified as shown in Eq. (13):

$$L_F(\boldsymbol{x}) = 1 - \Phi(\{\max[1 - F_S(\boldsymbol{x}, t=0), \min_{t\in(0,T]} F_S(\boldsymbol{x}, t) - 1] - \mu_\epsilon\}/\sigma_\epsilon \,|\, \boldsymbol{X} = \boldsymbol{x}) \quad (16)$$

If the time of the landslide initiation, t', is known, the observation event can be expressed with the factor of safety being equal to one at time t' with the following relation:

$$1 = F_S(\boldsymbol{x}, t=t') + \epsilon$$

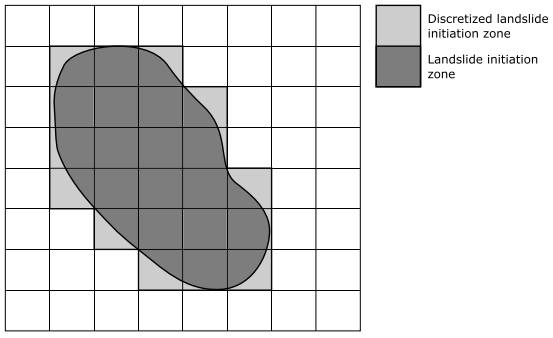

Fig. 1. Discretized landslide initiation zone.

Given that $F_S(\boldsymbol{x}, t = 0) \geqslant F_S(\boldsymbol{x}, t \in (0, T])$, this expression also satisfies the requirement that the slope is stable at the start of the rainfall event. For the same normal model error, the likelihood function can be specified as shown in Eq. (11):

$$L_F(\boldsymbol{x}) = \phi\left(\frac{1 - F_S(\boldsymbol{x}, t = t') - \mu_\epsilon}{\sigma_\epsilon}\middle| \boldsymbol{X} = \boldsymbol{x}\right) \tag{17}$$

For the cells that survived the rainfall event, this observation would correspond to the factor of safety being larger then one before and after the rainfall event.

$$Z_S = \{\boldsymbol{x} \in \mathbb{R}^n: 1 - \min_{t\in[0,T]} F_S\left(\boldsymbol{x}, t\right) \leqslant \epsilon\}$$

For the same normal model error, the likelihood function can be specified as shown in Eq. (13):

$$L_S(\boldsymbol{x}) = 1 - \Phi\left(\frac{1 - \min_{t\in[0,T]} F_S\left(\boldsymbol{x}, t\right) - \mu_\epsilon}{\sigma_\epsilon}\middle| \boldsymbol{X} = \boldsymbol{x}\right) \tag{18}$$

In this formulation, independence is assumed between the response of the soil and slope stability in the neighboring cells. This assumption is not necessarily realistic because of interactions that occur between the soil volumes in the neighboring cells at the cell interfaces. In terms of a hydro-mechanical soil response, these interactions involve transfer of normal and shear stresses, groundwater flow, and redistribution of surface water runoff. Except for the redistribution of the surface water runoff, these types of interactions are not integrated in majority of commonly used physical-based landslide prediction models. In addition to omitting potential interactions between the cells of the landslide models, this likelihood formulation does not take into account the effects of spatial dependency of model parameters, because the landslide model parameters are updated independently for each of the cells.

4.2.2. Full likelihood formulation

Accounting for the effects of spatial dependence in landslide model parameters would require the formulation of the joint likelihood function and modeling the triggering parameters as spatially dependent with a random field model. The joint likelihood formulation is obtained by combining all of the marginal cell-based likelihood functions in a single likelihood function. The joint likelihood function is obtained here by assuming independence between the observations of slope stability at each of the cells (i.e., slope failure or survival). Given that most of the landslide prediction models feature very weak or no interactions (e.g., redistribution of surface water runoff) between the neighboring cells, the assumption of independence between the cell-based likelihood function can be considered as reasonable when updating parameters of such models. However, it is important to note that the assumption of no interactions between the neighboring cells is not necessarily realistic.

Assuming that there are in total n_c cells in the landslide prediction model and that failure has been observed in n_F of the cells due to a rainfall event, while the remaining, $n_c - n_F$ cells were stable after the rainfall event. The joint likelihood function is formulated as follows:

$$L(\boldsymbol{x}) = \prod_{i=1}^{n_F} L_{Fi}(\boldsymbol{x}) \prod_{j=1}^{n_c - n_F} L_{Sj}(\boldsymbol{x}) \tag{19}$$

where $L_F(\boldsymbol{x})$ are the cell-based likelihood functions specifying the failure observations, as defined in Eqs. (16) and (17), and $L_S(\boldsymbol{x})$ are the cell-based likelihood functions specifying the survival observations, as defined in Eq. (18). Although formulating the joint likelihood function is relatively straightforward, evaluating it can be challenging due to the high dimensionality of the joint likelihood function. In the case of large numbers of cells-based observations, the value of the likelihood function can become very low and sometimes below the precision of the floating-point number format on computers. For example, the smallest positive usable number in the Python programming language module Numpy is around $2.23{\cdot}10^{-308}$ (The SciPy community, 2019), which would be exceeded in a situation with the likelihood of 1100 cell-based observations being 0.5. These considerations indicate that the joint cell-based likelihood function can be computationally intractable on problems with large observation sets.

4.2.3. Approximate likelihood formulation

One of the approaches to avoiding the computational difficulties with evaluating the full likelihood is the implementation of an approximate likelihood function. The development of an approximate likelihood function is based on the Approximate Bayesian Computation (ABC) method (e.g., Sisson et al., 2018). In the ABC method, a lower-dimensional likelihood function is formulated based on summary statistics to avoid computational difficulties of the higher-dimensional full likelihood. The approximate likelihood function is formulated by measuring the discrepancy between a chosen set of statistics of the model output and the corresponding estimates from the observations. The summary statistics is often represented by the mean and standard deviation, such that the updating process aims to minimize the discrepancy between the summary statistics calculated from the model output and the observations.

The formulation of the approximate likelihood function and the selection of the summary statistics will be adapted to the problem of updating parameters of a physical-based landslide prediction model. The development of the approximate likelihood formulation will be examined with respect to the landslide initialization process, as illustrated in Fig. 1. In the case of the marginal and the joint likelihood function, the observation of landslide initiation within a single initiation zone is interpreted as a value of the factor of safety being equal or lower than one for all of the cells within the initiation zone.

However, the landslide initiation process is often more complex and involves the development of an initial weak soil zone and its propagation prior to landsliding. This process is commonly referred to as the shear band propagation mechanism, where the shear band is a thin zone of intense shearing. The formation of the initial weak zone can occur as a combinations of various factors including, among others, additional loading, loss of suction due to the wetting process, added weight from the increased soil saturation, groundwater flow, surface erosion and deposition, internal erosion and piping, and artesian pressure from the rock base. Following the formation of the initial weak zone, the propagation of the shear band occurs as the soil in the initially zone is not capable of withstanding the loads acting on it. The excess loads are then distributed to the neighboring, initially stable, soil zones. If the excess loads surpass the capacity of the neighboring soil zones to sustain the additional loads, the redistribution of loads leads to the propagation of the shear band along the slope. Consequently, this leads to the initiation of a landslide with the detachment of soil from the slope. Additional challenges occur in strain-softening materials, where the soil shear strength decreases to a residual value from the peak after the shear strains reach certain critical value. Shear band propagation starts in an initially weak zone of the slope as the shear strength reduces due to the softening behavior of the material in the band. The shear band continues to propagate further from the initial zone due to the redistribution of excess loads. Finally, the propagation of the shear band causes landsliding with the detachment of the unstable soil from the slope.

Not accounting for the redistribution of loads and the propagation of the shear band can lead to a significant underestimation of the landslide volume (e.g., Kim et al., 2018). This observation becomes important in relating the observation of a landslide initiation zone to the corresponding prediction with a physical-based landslide prediction model. Commonly employed landslide prediction models evaluate the stability of a slope on a cell basis, such that the stability of each of the cell is evaluated independently without a mechanism to propagate the

shear band. The interpretation of an observation of a landslide initiation zone as a model prediction with a factor of safety lower or equal to one in each of the cells of the discretized initiation zone is not the necessary requirement due to the effect of shear band propagation. Conversely, landslide initiation in the observed zone can also occur through shear band propagation that starts from a weak zone formed in a sub-area of the zone. This observation can be interpreted as a requirement that a subset of the cells in the discretized landslide initiation area needs to have a factor of safety lower or equal to one.

The development of an approximate approach is considered here due the absence on an explicit approach for the shear band propagation in the commonly used landslide prediction models. Approximate expressions can be obtained by relating the global factor of safety over the initiation zone, F_S^g, to the factors of safety of cells within the initiation zone, $\{F_{Si},\, i = 1,...,n_i\}$. In general, F_S^g is defined as a ratio of the global resisting forces, R_g, and the driving forces, S_g, along the critical failure plane within the landslide initiation zone. An approximate formulation can be derived by expressing R_g as the sum of the resisting forces, $\{R_i,\, i = 1,...,n_i\}$ of the grid cells in the initiation zone, while S_g is expressed as the sum of the corresponding driving forces, $\{S_i,\, i = 1,...,n_i\}$. If the sums of the resistance and the driving forces across the cells are expressed with the respective arithmetic mean values, $\overline{R}$ and $\overline{S}$, F_S^g can be related to the arithmetic average of the factors of safety of cells within the initiation zone, $\overline{F}_S$, as shown in Eq. (20). It is important to note that the expression in Eq. (20) represents a very simple approximation of F_S^g as the load and resistance forces are vector values, while the approximation is based on the arithmetic sum of forces instead of the vector sum. Additionally, the formulation does not account for the complexities of the landslide propagation process (e.g., redistribution of forces and landslide propagation).

$$F_S^g(\boldsymbol{x},\, t) = \frac{R_g}{S_g} \approx \frac{\sum_{i=1}^{n_i} R_i}{\sum_{i=1}^{n_i} S_i} = \frac{n_i \overline{R}}{n_i \overline{S}} = \frac{\overline{R}}{\overline{S}} = \overline{F}_S = \frac{1}{n_i}\sum_{i=1}^{n_i} F_{Si}(\boldsymbol{x},\, t)$$
$$= A\left[F_{Si}(\boldsymbol{x},\, t)\colon i = 1,...,n_i\right] \tag{20}$$

The presence of heterogeneity in the triggering parameters of landslides introduces additional challenges in understanding and approximating the landslide propagation process. The effects of heterogeneity in soil properties on the stability of slopes have been examined in numerous studies (e.g., Fenton and Griffiths, 2008; Depina and Wolebo, 2017). Some of the most important observations in those studies relate to effects of heterogeneity on the propagation of the failure surface and the importance of low values of the soil strength on the estimated factor of safety. Heterogeneity affects the development of the failure surface, such that the failure surface develops and propagates along the weakest path with low shear strength values (Fenton and Griffiths, 2008). Based on those findings, it was demonstrated empirically in Fenton and Griffiths (2008) that the harmonic average is best suited to characterize the effects of the heterogeneous shear strength values on the stability of a slope. This is explained by the harmonic average being dominated by the low values, which is similar to the development of the failure surface in slopes following the path of low-strength areas. This finding is applied here by considering approximation of F_S^g with a harmonic average of the factors of safety of cells within the initiation zone, as specified in Eq. (21). Unlike the expression in Eq. (20), the authors were not able to provide a more direct relation between F_S^g, with the expression being based only on the empirical observations.

$$F_S^g(\boldsymbol{x},\, t) = \frac{R_T}{S_T} \approx \Theta\left[F_{Si}(\boldsymbol{x},\, t)\colon i = 1,...,n_i\right] = \left[\frac{\sum_{j=1}^{n_i} F_{Sj}(\boldsymbol{x},\, t)^{-1}}{n_i}\right]^{-1} \tag{21}$$

Some of the limitations in the derivation of the approximate F_S^g in Eqs. (20) and (21) can be alleviated by implementing more advanced landslide prediction models (e.g., finite element or finite difference coupled hydro-mechanical models). Implementation of models that are able to explicitly satisfy the force equilibrium and simulate the landslide propagation process would provide a more consistent evaluation of F_S^g. However, more advanced models are not commonly implemented on scales larger than a single slope due to, among others, large computational demands, high sensitivity to changes in model parameters, and issues with numerical stability. Additional assumption includes vertically discontinuous failure surface across the initiation zones, which is a consequence of the grid cell discretization of the implemented landslide prediction model and varying depths to bedrock across cells. Motivated by these challenges, the implemented approximations of F_S^g in Eqs. (20) and (21) are developed based on modeling features incorporated in the state-of-the-art physical-based landslide prediction models with their inherent limitations as stated earlier.

The approximations of F_S^g in Eqs. (20) and (21) are used as summary statistics to develop approximate likelihood formulations. Let us consider a landslide initiation zone in a subset of grid cells in the landslide model discretization, $C_i \subseteq C$, where C is the set of n_C cells indexed from 1 to n_C.

For a landslide initiation zone, C_i, this observation event can be expressed with the arithmetic or harmonic mean of the factors of safety within the zone as greater than one at the start of the rainfall event, and equal to or lower than one after the rainfall event. The corresponding observation event and the likelihood function for the arithmetic mean are defined as follows:

$$Z_{Fi}^A = \{\boldsymbol{x} \in \mathbb{R}^n\colon g_A(\boldsymbol{x}) = \max[1 - A(F_{Sj}(\boldsymbol{x},\, t = 0)\colon j \in C_i),\ \min_{t\in(0,T]} A(F_{Sj}(\boldsymbol{x},\, t)\colon j \in C_i) - 1] \leqslant \epsilon\} \tag{22}$$

$$L_{Fi}^A(\boldsymbol{x}) = 1 - \Phi\left(\frac{g_A(\boldsymbol{x}) - \mu_\epsilon}{\sigma_\epsilon}\middle|\boldsymbol{X} = \boldsymbol{x}\right) \tag{23}$$

For a landslide initiation zone where the time of initiation, t', is known, the observation event can be expressed with the arithmetic or harmonic means of the factors of safety within the zone being equal to one at time t'. The formulation for the observation event specified by the arithmetic mean follows:

$$1 = A(F_{Sj}(\boldsymbol{x},\, t = t')\colon j \in C_i) + \epsilon$$

The likelihood function is formulated as:

$$L_{Fi}^A(\boldsymbol{x}) = \phi\left(\frac{1 - A(F_{Sj}(\boldsymbol{x},\, t = t')\colon j \in C_i) - \mu_\epsilon}{\sigma_\epsilon}\middle|\boldsymbol{X} = \boldsymbol{x}\right) \tag{24}$$

The spatial correlation is incorporated in the likelihood formulations by considering the model parameters as correlated through the random field model. For a subset of cells where no landslide initiation was observed during the rainfall event, $C_{Si} \subseteq C$, the approximate likelihood function can be derived from an observation event where the arithmetic or harmonic mean of the factor of safety in those cells is larger then one before and during the rainfall event. For the case of the arithmetic mean, the observation event is defined as:

$$Z_{Si}^A = \{\boldsymbol{x} \in \mathbb{R}^n\colon 1 - \min_{t\in[0,T]} A\left(F_{Sj}\left(\boldsymbol{x},\, t\right)\colon j \in C_{Si}\right) \leqslant \epsilon\}$$

The likelihood function can be specified as follows:

$$L_{Si}^A(\boldsymbol{x}) = 1 - \Phi\left(\frac{1 - \min_{t\in[0,T]} A\left(F_{Sj}\left(\boldsymbol{x},\, t\right)\colon j \in C_{Si}\right) - \mu_\epsilon}{\sigma_\epsilon}\middle|\boldsymbol{X} = \boldsymbol{x}\right) \tag{25}$$

Similarly, the corresponding observation event and the likelihood functions for the harmonic case in Eqs. (23)–(25) would be specified by replacing A with Θ, as defined in Eq. (21).

In the case of large number of stable cells, spanning large spatial distances, the approximate likelihood formulation can be refined by subdividing those cells into a number mutually exhaustive zones, $C_{S1} \cup C_{S2} \cup ... \cup C_{SN_S} = C_S$, and specifying an approximate likelihood function for each of the zones.

The joint approximate likelihood function is formulated by assuming independence between the observation events in each of the landslide initiation zones and the zones where no initiation was observed during the rainfall. This is not a very strong assumption (i.e., close to reality) for the initiation zones as they are non-overlapping and the interactions between the different initiation zones are not likely to significantly affect the stability of those zones. The assumption of independence is stronger (i.e., less realistic) between the landslide initiation zones and the stable zones and among the stable zones because strong interactions that affect the stability of those zones cannot be excluded.

Assuming that the landslide initiation zones are discretized into N_i initiation zones, C_{Fi}, $i = 1, ..., N_i$, with the stable zones discretized into N_s zones, C_{Si}, $i = 1, ..., N_s$, the approximate likelihood function is specified as follows:

$$L_A(\boldsymbol{x}) = \prod_{i=1}^{N_i} L_{Fi}^A(\boldsymbol{x}) \prod_{j=1}^{N_s} L_{Sj}^A(\boldsymbol{x}) \tag{26}$$

5. Analytical example

5.1. Problem formulation

A relatively simple and reproducible Bayesian updating problem is implemented to illustrate the performance of the proposed approximate likelihood formulations with the BUS algorithm. The problem examines updating of uncertainties associated with a simplified spatially distributed landslide prediction model. The landslide prediction model is implemented on a domain of 90 × 90 m. The domain is discretized in a grid of 9 × 9 equally-sized cells indexed $\{(i, j) \in D: i = 0, ..., 8, j = 0, ..., 8\}$, as shown in Fig. 2.

The stability of each of the cells is evaluated independently based on the value of the factor of safety, F_S. The following relation for F_S is implemented to obtain a relatively simple formulation of the updating problem:

$$F_S(\boldsymbol{R}) = \boldsymbol{R} \tag{27}$$

where $\boldsymbol{R}$ is a spatially variable model parameter that accounts for the effects of uncertainties in landslide model parameters (e.g., slope angle, depth to bedrock, strength parameters) on the slope stability. Stability of each of the cells in the model is evaluated based on the value of F_S, such that a cell (i, j) is stable if $F_{Si,j} > 1$ and unstable if $F_{Si,j} \leqslant 1$.

Based on the problem formulation, a reliability problem can be

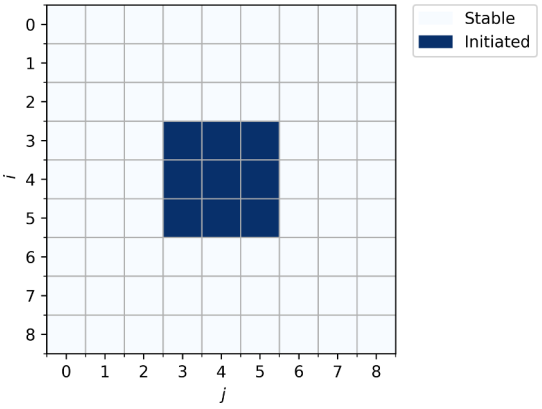

Fig. 2. Discretization of the model domain with the cells corresponding to the landslide initiation zone highlighted.

defined to estimate the probability of landslide initiation for each of the cells. For a cell (i, j), the reliability problem is defined with the following performance function:

$$g_{i,j}(\boldsymbol{R}, \epsilon_M) = F_{Si,j}(\boldsymbol{R}) + \epsilon_M - 1 \tag{28}$$

where ϵ_M is the model error. The probability of landslide initiation or failure probability in a cell (i, j) is defined as:

$$P_{Fi,j} = P(g_{i,j}(\boldsymbol{R}, \epsilon_M) \leqslant 0) \tag{29}$$

5.2. Prior

Uncertainties in the values of $\boldsymbol{R}$ are modeled with a Gaussian random field to account for the spatial dependence in the parameters controlling the slope stability. The random field model discretization follows the one of the domain D, with the mid-point method used to calculate the elements of the covariance matrix. The prior values of $\boldsymbol{R}$ are defined with constant mean of $\mu'_{\boldsymbol{R}} = 1.3$ and standard deviation of $\sigma'_{\boldsymbol{R}} = 0.2$ over the model domain. Spatial dependence is modeled with the ellipsoidal autocorrelation model with $l_x = l_y = 50$ m. Uncertainties associated with $\boldsymbol{R}$ are considered as reducible in the updating process. The model error is assumed to be normally distributed, $\epsilon_M \sim N(0, \sigma_M)$ with $\sigma_{\epsilon_M} = 0.05$, and non-reducible in the updating process.

Given that $\boldsymbol{R}$ and ϵ_M are normally distributed, the statistical properties of g in Eq. (28) can be analytically calculated with $g \sim N(\mu_g, \sigma_g)$, where $\mu_g = \mu_{\boldsymbol{R}} - 1$ and $\sigma_g = \sqrt{\sigma_{\boldsymbol{R}}^2 + \sigma_{\epsilon_M}^2}$. The prior failure probability, P'_F, is equal for all of the cells and can be calculated as follows:

$$P'_F = P\left(g \leqslant 0\right) = P\left(\frac{g - \mu_g}{\sigma_g} \leqslant -\frac{\mu_g}{\sigma_g}\right) = \Phi\left(-\frac{\mu_g}{\sigma_g}\right) = \Phi\left(-1.455\right) = 7.281 \cdot 10^{-2} \tag{30}$$

5.3. Likelihood function

The likelihood function will be derived from the approximate likelihood formulations in Section 4.2.3 with the time omitted from those equations as the problem does not feature the time component. The initiation zone is associated with the subdomain of $F \subset D$, and specified with the following cell indices $\{(i, j) \in F: 3 \leqslant i \leqslant 5, 3 \leqslant j \leqslant 5\}$. The slope cells that remained stable are associated with the domain $S \subset D$, such that $S \cap F = \varnothing$ and $S \cup F = D$. The effects of different likelihood formulations on the posterior distributions will be examined by considering the following cases:

- Case 1: Likelihood formulation in Eq. (23) for the initiation zone and in Eq. (25) for the stable zone with both the arithmetic and harmonic means for F_S^g. The likelihoods for the arithmetic mean are specified as follows:

$$L_F^A(\boldsymbol{r}) = 1 - \Phi\left(\frac{A(F_{Si,j}(\boldsymbol{r}): (i, j) \in F) - 1}{\sigma_{\epsilon_M}} \,\middle|\, \boldsymbol{R} = \boldsymbol{r}\right) \tag{31}$$

$$L_S^A(\boldsymbol{r}) = 1 - \Phi\left(\frac{1 - A(F_{Si,j}(\boldsymbol{r}): (i, j) \in S)}{\sigma_{\epsilon_M}} \,\middle|\, \boldsymbol{R} = \boldsymbol{r}\right) \tag{32}$$

- Case 2: Likelihood formulation in Eq. (24) for the initiation zone and in Eq. (25) for the stable zone with both the arithmetic and harmonic means for F_S^g. The likelihoods for the arithmetic mean are specified as follows:

$$L_F^A(\boldsymbol{r}) = \phi\left(\frac{1 - A(F_{Si,j}(\boldsymbol{r}): (i, j) \in F)}{\sigma_{\epsilon_M}} \,\middle|\, \boldsymbol{R} = \boldsymbol{r}\right) \tag{33}$$

$$L_S^A(\boldsymbol{r}) = 1 - \Phi\left(\frac{1 - A(F_{Si,j}(\boldsymbol{r}): (i,j) \in S)}{\sigma_{\epsilon_M}} \,\middle|\, \boldsymbol{R} = \boldsymbol{r}\right) \tag{34}$$

The approximate likelihood function is specified as follows:

$$L_A(\boldsymbol{r}) = L_F^A(\boldsymbol{r}) L_S^A(\boldsymbol{r})$$

Expression for the harmonic mean would be specified by replacing A with Θ in Eqs. (31)–(34).

5.4. Posterior

Given the prior knowledge and the likelihood functions, the BUS algorithm was implemented to obtain $K = 10^5$ samples from the posterior distribution. Samples from the posterior distributions were also used to update the reliability estimates and evaluate the effects of the observations on the slope stability assessment.

5.5. Case 1

The results of the updating process for Case 1 are presented in Figs. 3–5. Fig. 3(a) and (b) present the posterior mean, $\mu''_{\boldsymbol{R}}$, and standard deviation, $\sigma''_{\boldsymbol{R}}$, respectively, where the arithmetic mean was used for F_S^g. From Fig. 3(a), it can be observed that the values of $\mu''_{\boldsymbol{R}}$ within cells of the initiation zone are close to or lower than one, corresponding to the observation that F_S^g in the initiation zone is lower or equal to one. The values of $\mu''_{\boldsymbol{R}}$ in the cells of the stable zone are below the prior mean of $\mu'_{\boldsymbol{R}} = 1.3$ and increase from around 1 to 1.25 as the distance from the initiation zone increases. This is a consequence of the spatial dependence between the values of $\boldsymbol{R}$, as specified by the Gaussian random field model.

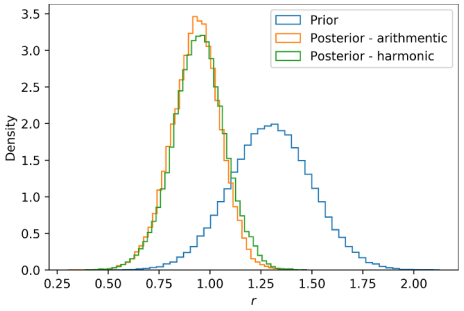

Fig. 4. Prior and posterior distributions of R at cell (4, 4) based on the arithmetic and harmonic mean for F_S^g.

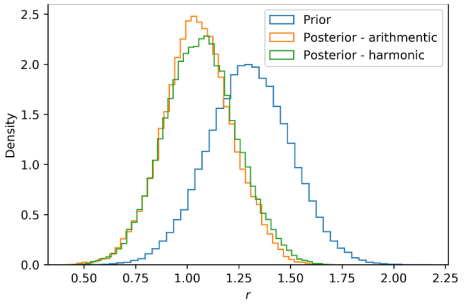

Fig. 5. Prior and posterior distributions of R at cell (2, 4) based on the arithmetic and harmonic mean for F_S^g.

The effects of updating on the values of $\sigma''_{\boldsymbol{R}}$ can be examined in Fig. 3(b). The values of $\sigma''_{\boldsymbol{R}}$ within the cells of the initiation zone are reduced from the prior value of $\sigma'_{\boldsymbol{R}} = 0.2$ to approximately below 0.15. The values of $\sigma''_{\boldsymbol{R}}$ increase in the cells of the stable zone from 0.15 to 0.2

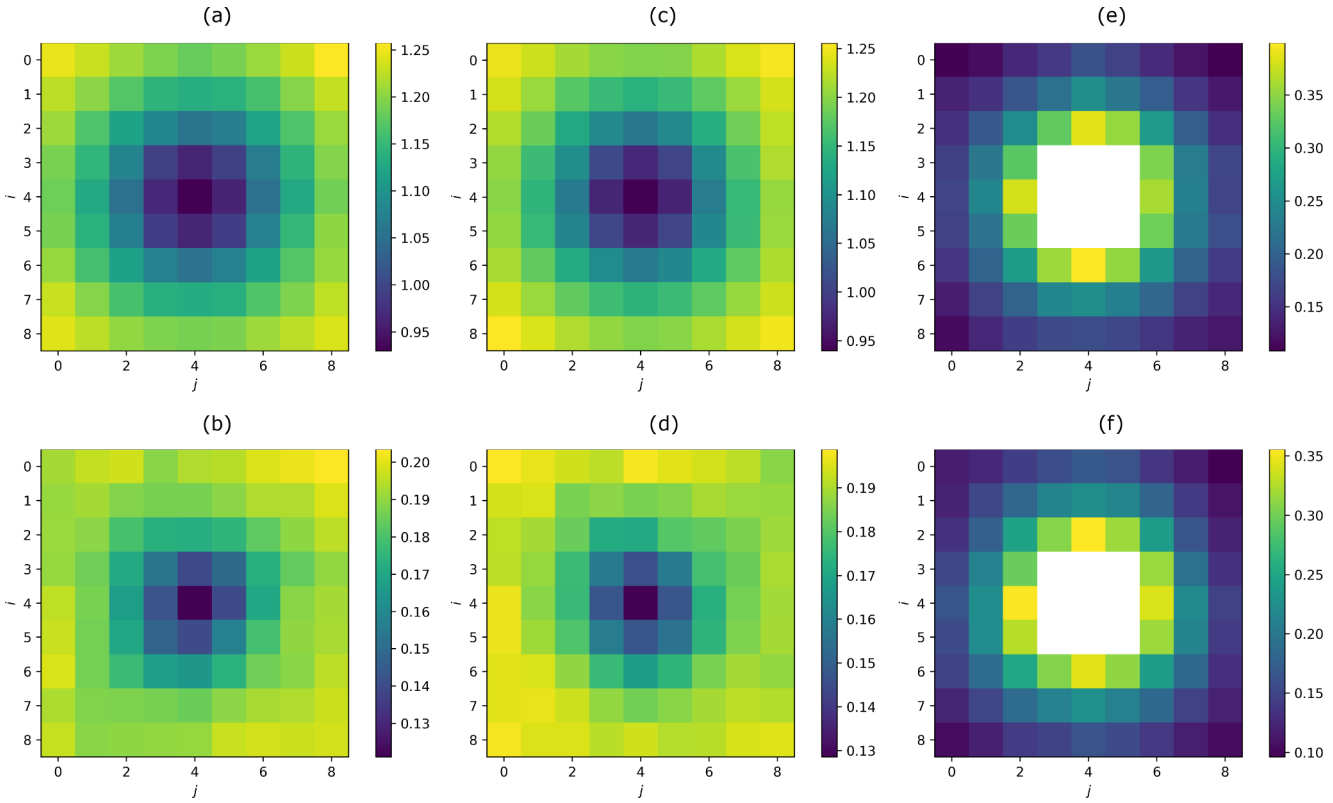

Fig. 3. Case 1: (a) Posterior mean of $\boldsymbol{R}$ based on the arithmetic mean for F_S^g, (b) Posterior standard deviation of $\boldsymbol{R}$ based on the arithmetic mean for F_S^g, (c) Posterior mean of $\boldsymbol{R}$ based on the harmonic mean for F_S^g, (d) Posterior standard deviation of $\boldsymbol{R}$ based on the harmonic mean for F_S^g, (e) Posterior failure probability, P''_F based on the arithmetic mean for F_S^g, (f) Posterior failure probability, P''_F based on the harmonic mean for F_S^g.

as the distance from the initiation zone increases. The observed variations in the values of $\sigma''_{\boldsymbol{R}}$ within the stable zone are due to the effects of spatial variability in the values of $\boldsymbol{R}$. Additionally, based on the stronger reduction of $\sigma''_{\boldsymbol{R}}$ in the initiation zone, it can be detected that the observation of slope instability represents a stronger information than the observation of a stable zone in this case as it allows for a larger reduction of uncertainties. Slightly non-symmetric appearance of the results in Fig. 3(b) is due to a limited number of samples. Similar observation can be made for the results of updating process where F_S^g was calculated with the harmonic mean that are presented in Fig. 3(c) and (d).

Fig. 3(e) and (f) present the posterior failure probabilities, P''_F in the cells of the stable zone. The values of for a cell (i, j) are calculated based on the following expression to account for the model error:

$$P''_{Fi,j} = \frac{1}{K}\sum_{i=1}^{K} \Phi\left(\frac{1 - F_{Si,j}(\boldsymbol{r}'') - \mu_{\epsilon_M}}{\sigma_{\epsilon_M}}\right) \tag{35}$$

The cells in the initiation zone are omitted from the analysis as failure had already occurred in those cells. From Fig. 3(e) and (f) it can be observed that the observation of an initiation zone resulted in increased posterior failure probabilities, P''_F within the cells of the stable zone. The values of P''_F range from the prior probability of $P'_F = 7.281{\cdot}10^{-2}$ to values greater than 0.35, which represents an increase in failure probability on the magnitude of five times. The increase in the failure probability decays with the distance from the initiation zone, with the highest probabilities observed in cells neighboring the initiation zone.

Additionally, histograms of the posterior distributions of $\boldsymbol{R}$ at selected cells in the model are presented to investigate potential differences between the arithmetic and harmonic formulations for F_S^g on the updating results. Fig. 4 presents the prior and posterior distributions for the two F_S^g formulations at the cell (4, 4) in the initiation zone. Conversely, Fig. 5 presents the prior and posterior distributions for the two F_S^g formulations at the cell (2, 4), which is in the stable zone and in close proximity to the initiation zone.

From Fig. 4 it can be observed the mean values of the two posterior distributions are below one, corresponding to the observation of an unstable zone. The comparison of the two posterior distributions reveals that the distribution for the arithmetic formulation of F_S^g is slightly narrower with a lower mean value than the distribution for the harmonic formulation of F_S^g. This can be explained by the harmonic mean being dominated by the lower values. Similar observation can be made for the posterior distributions for the cell (2, 4) in the stable zone, with the main difference being that the distributions have mean values around one or greater. For the remaining cells in the stable zone, similar observations apply with the mean values increasing as the distance from the initiation zone increases.

5.6. Case 2

The results of the updating process for Case 2 are presented in Figs. 6–8. Similar trends are observed as for Case 1, with the focus of the presentation in the following paragraphs being on the difference between Cases 1 and 2. A comparison of the corresponding results from the analyses in Cases 1 and 2 shows that the reduction of $\mu''_{\boldsymbol{R}}$ values in the initiation zone for Case 1 is stronger due to the observation being understood as $F_S^g \leqslant 1$ rather than $F_S^g = 1$ for Case 2. The comparison of $\sigma''_{\boldsymbol{R}}$ values reveals that the reduction in standard deviations in the initiation zone is stronger for Case 2 than for Case 1. This is explained by the information on slope initiation in Case 2, defined as $F_S^g = 1$, providing stronger information that leads to a greater reduction in uncertainties than $F_S^g \leqslant 1$ in Case 1. The comparison of the estimated P''_F for the Cases 1 and 2 shows that higher probabilities are obtained for the Case 1. This observation is consistent with the earlier observations on the differences in the posterior distributions between Cases 1 and 2. Higher P''_F are a consequence of the interpretation of the observation event in Case 1 leading to lower values of $\mu''_{\boldsymbol{R}}$ with similar values of $\sigma''_{\boldsymbol{R}}$ in the cells of the stable zone.

The properties of the posterior distribution of $\boldsymbol{R}$ are further investigated with histograms at several cells in the model in Figs. 7 and 8. The comparison of the posterior distributions in the initiation zone for the analyses in Cases 1 and 2 shows that the posterior distributions for Case 2 have a mean closer to one and a lower variability around the mean than the posterior distributions in Case 1. In the stable zone, similar values of standard deviation are observed with the means being slightly higher for Case 2 due to higher means in the initiation zone.

In addition to the analytical example, a relatively simple Bayesian updating problem is implemented in Appendix B on a simplified TRIGRS model. The reader is advised to examine the Bayesian updating results in Appendix B for a more straightforward interpretation of the results of the Kvam case study in Section 6.

6. Kvam case study

The capacity of the methodology in integrating observations into spatially variable models of uncertain soil parameters will be investigated on the Kvam case study. Kvam is a town in the central southern Norway, within the Gudbrandsdalen valley. The Gudbrandsdalen valley has been carved by glaciers, featuring steep edges covered with glacial deposits, as shown in Fig. 9. From Fig. 9 it can be observed that the area under Kvam and the valley base are characterized by fluvial deposits with pockets of glaciofluvial deposits. Hill sides rising above the valley base are covered with moraine or glacial deposits, transitioning from thick to thin moraine cover as the height increases. Subcropping bedrock with a thin cover of humus or peat is usually found above the areas covered with thin moraine deposits.

The area surrounding Kvam is prone to various types of geohazards including shallow landslides, debris flow and rock fall. This is witnessed by the presence of deposits at the base of many slopes and visible landslide scars, as indicated in Fig. 9. The focus of this study will be on the landslides following the rainfall events that occurred in 2011 and 2013, presented in Fig. 14. These rainfall events caused flooding of the town and multiple landslides on the surrounding hills. Among the locations affected by landslides, the area indicated in Fig. 9 was selected for a detailed analysis due to relatively high density of landslides during these events. More detailed information on the conditions prior and after the landslide events is presented in aerial photos in Figs. 10–12.

Fig. 10 presents an aerial photo of the studied area prior to the landslide events in 2010. As observed in Fig. 10, the slope areas are covered with vegetation with some indications of channels along the slope with relatively denser vegetation. The conditions at the studied area after the landslide events in 2011 can be interpreted from Fig. 11. Following the rainfall even between June 9th and 10th of 2011 with the total rainfall of 61.72 mm/day, several landslides were observed in the hills near Kvam. A set of landslide scars can be clearly identified from Fig. 11 due to the missing vegetation and deposited soil masses at the base of the slope.

Approximately two years after the landslide events of 2011, an intense rainfall caused flooding and initiation of landslides in the areas surrounding Kvam on May 23rd 2013. An aerial photo of the studied area after the event on May 23rd 2013 is presented in Fig. 12. A new landslide scar can be observed in the lower part of Fig. 12 in addition to the ones from 2011. From the spread of deposits at the base of the slope, it can be detected that the scars activated in 2011 were relatively inactive during the 2013 event. This can be further confirmed by comparing the distribution of the spread after the events of 2011 and 2013 in Figs. 11 and 12. This is attributed to the relatively low surface cover on the slope scars from 2011 with higher resistance to landsliding due to relatively higher effects of cohesion and vegetation on the slope stability.

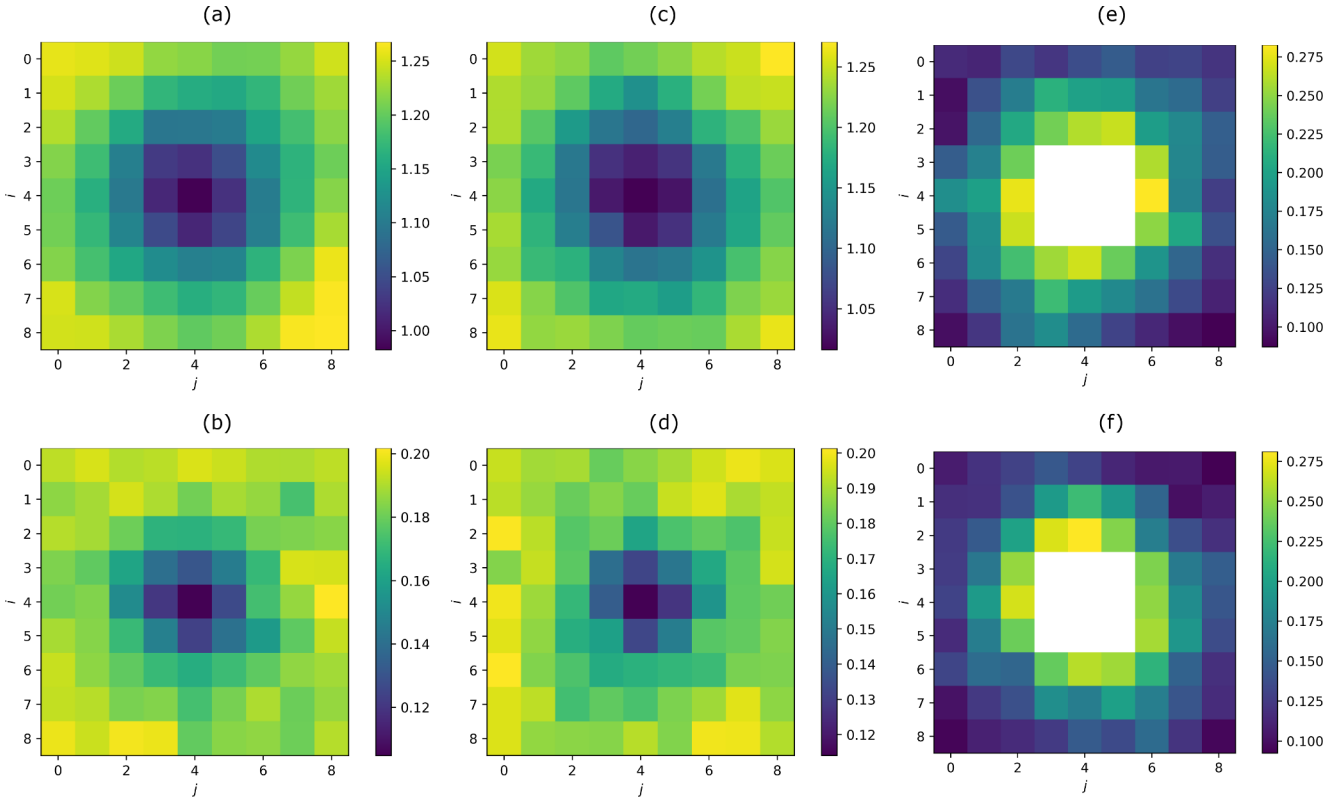

Fig. 6. Case 2: (a) Posterior mean of $\boldsymbol{R}$ based on the arithmetic mean for F_S^g, (b) Posterior standard deviation of $\boldsymbol{R}$ based on the arithmetic mean for F_S^g, (c) Posterior mean of $\boldsymbol{R}$ based on the harmonic mean for F_S^g, (d) Posterior standard deviation of $\boldsymbol{R}$ based on the harmonic mean for F_S^g, (e) Posterior failure probability, P_F'' based on the arithmetic mean for F_S^g, (f) Posterior failure probability, P_F'' based on the harmonic mean for F_S^g.

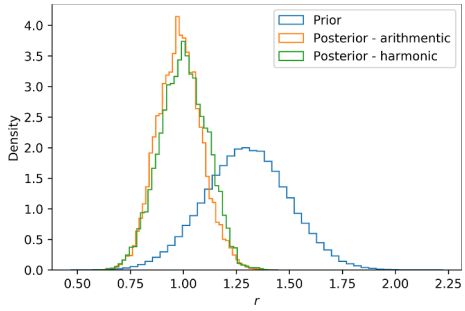

Fig. 7. Prior and posterior distributions of R at cell (4, 4) based on the arithmetic and harmonic mean for F_S^g.

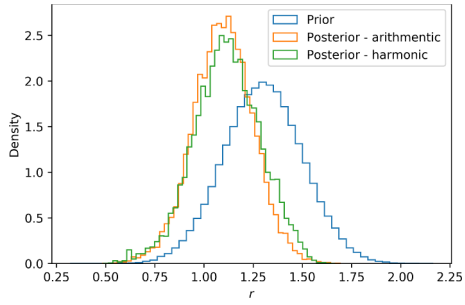

Fig. 8. Prior and posterior distributions of R at cell (2, 4) based on the arithmetic and harmonic mean for F_S^g.

6.1. Prior information

Information on the topography of the studied area is based on a 10 x 10 m digital elevation model (DEM), as presented in Fig. 13. The depth

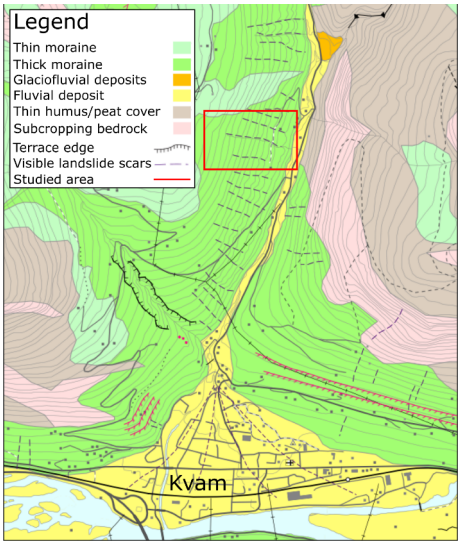

Fig. 9. Quaternary map of the are surrounding Kvam. Adapted and modified based on information from NGU (2019).

to bedrock, H, was determined based on field data from Holm (2011) and Edvardsen (2013), and the comparison of high quality DEM models before and after the landslides. The following relationship between H and the tangent of the slope angle, $\tan(\delta)$ is determined empirically from the collected data:

$$H = \max\{H_{\min}, \mu_H + \epsilon_H\} \tag{36}$$

where $H_{\min} = 0.4$ m is the minimal depth to bedrock, $\mu_H = -2.578 \cdot \tan(\delta) + 2.612$ is the mean defined by a linear trend function and $\epsilon_H \sim N(0, \sigma_H) = N(0, 0.271)$ is the residual around the

Fig. 10. Aerial photo of the studied area in Kvam, central Norway, in 2010. Source: norgeibilder.no.

Fig. 11. Landslide events within the studied area on June 10th 2011. Source: norgeibilder.no.

Fig. 12. Landslide events within the studied area on May 23rd 2013. Source: norgeibilder.no.

trend. The minimum value of $H_{\min}$ is imposed as the lowest thickness value measured in the field to characterize the surficial cover of glacial environments for the highest slope values. Spatial dependence of H and H_w is not explicitly modeled due to the strong dependence of H to the local variations of δ.

Geotechnical and hydraulic parameters of the TRIGRS model will be considered as uncertain due to the natural variability characteristic for these parameters and the lack of field investigations and laboratory tests that would contribute to reducing the uncertainties. The parameters of the distributions describing the uncertainties in the parameters are selected from literature sources to be relevant for the considered soil type, as presented in Table 1. Spatial variability of geotechnical and hydraulic parameters is modeled with normal and lognormal random field models. The random field models are discretized based on the DEM representation of the studied domain. The spatial dependency of parameters in the lateral directions is specified by the ellipsoidal autocorrelation function with the correlation lengths in both horizontal directions of 50.0 m. Horizontal correlation lengths are

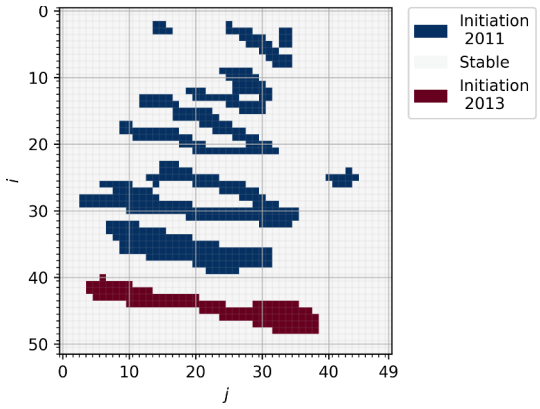

Fig. 13. DEM discretization of the studied domain with the initiation zones for the landslide events of 2011 and 2013.

selected within the ranges characteristic for several geotechnical parameters reported in Phoon and Kulhawy (1999).

The remaining geotechnical and hydraulic input parameters to TRIGRS were modeled as deterministic as they were not significantly affected during the updating process. The following deterministic values were adopted for relative dry density, $G_s = 2.7$, void ratio, $e = 0.26$, saturated, $\theta_s = 0.4$ and residual, $\theta_r = 0.05$, volumetric water contents.

Given the problem definition and the specification of model parameters, the prior knowledge is defined in terms of the joint distribution of the uncertain model parameters, $\boldsymbol{X} = [c, \phi, H, H_w, k_s, D_0]^T$, where $\boldsymbol{X}$ is the vector of model parameters with c, ϕ, H, H_w, k_s, D_0 being spatially variable parameters discretized over the study domain. The vector of model parameters is distributed according to prior joint pdf such that $\boldsymbol{X} \sim f'_{\boldsymbol{X}}(\boldsymbol{x})$.

6.2. Likelihood function

The likelihood function will be derived by following the approximate likelihood formulations based on the observations of landslide initiation zones for a given rainfall. The initiation zones are discretized with respect to the adopted DEM map, as shown in Fig. 13. In addition to the zones that remained stable after the rainfall events, the studied area is classified into zones where slope initiations were observed after the landslide events of 2011 and 2013, respectively. The classification of the zones with respect to the time of occurrence is important for a consistent implementation of the updating process. The runnout zones were not included in the analyses as the TRIGRS software does not account for the post-failure behavior of soil masses.

Meteorological observations in this study consists of two rainfall events on June 10th 2011 and May 23rd 2013, as presented in Fig. 14. Hourly measurements of rainfall intensities for the two events are presented side-by-side in Fig. 14 within a period of 24 h. Note that the horizontal axis represents time since the start of the analyzed 24-h periods and not the time of the day for the two events. In addition to the measured values, average rainfall intensities within the studied 24-h periods for the two events are presented. The average rainfall intensity for the rainfall event in 2011 is $\bar{I}_{Z,2011} = 2.572$ mm/h $= 61.72$ mm/day. The average rainfall rate for the rainfall event in 2013 is slightly lower and equal to $\bar{I}_{Z,2013} = 2.107$ mm/h $= 50.56$ mm/day. To simplify the implementation of the TRIGRS model, the average rainfall intensities are simulated over the studied 24-h periods in 2011 and 2013 instead of the measured values.

Prediction accuracy of TRIGRS is modeled by the model error, ϵ_M. The model error is assumed to follow a normal distribution with zero-mean and standard deviation of $\sigma_{\epsilon_M} = 0.05$. The standard deviation value is selected based on the study by Duncan and Wright (1980). σ_{ϵ_M} relates only to the model error in the slope stability model and it does not include errors in the infiltration model. The uncertainties in ϵ_M are

Table 1
Distributions of uncertain model parameters.

Parameter		Distribution	Distribution parameters		Source
H [m]	Depth to bedrock	Lognormal	$\mu_H = -2.578\cdot\tan(\theta) + 2.612$	$\sigma_H = 0.271$	–
c [kPa]	Cohesion	Lognormal	$\mu_c = 4.0$	$\mathrm{CoV}_c = 0.3$	Mean value adapted from Melchiorre and Frattini (2012). Coefficient of variation based on Lacasse and Nadim (1996).
ϕ [°]	Friction angle	Normal	$\mu_\phi = 32.0$	$\mathrm{CoV}_\phi = 0.2$	Mean and coefficient of variation adapted from Melchiorre and Frattini (2012).
H_w [m]	Initial water depth	Uniform	$H_{w,\min} = 0.0$	$H_{w,\max} = H$	–
k_s [m/s]	Saturated coefficient of permeability	Lognormal	$\mu_{K_s} = 1.0\cdot10^{-6}$	$\mathrm{CoV}_{k_s} = 1.0$	Mean based on the values from Melchiorre and Frattini (2012) and Janbu et al., 1989.
D_0 [m^2/s]	Diffusivity	Lognormal	$\mu_{D_0} = 5.0\cdot10^{-6}$	$\mathrm{CoV}_{D_0} = 1.0$	Mean based on the values from Melchiorre and Frattini (2012).
ϵ_M	Slope stability model error	Normal	$\mu_{\epsilon_M} = 0.0$	$\sigma_{\epsilon_M} = 0.05$	Standard deviation value from Duncan and Wright (1980).

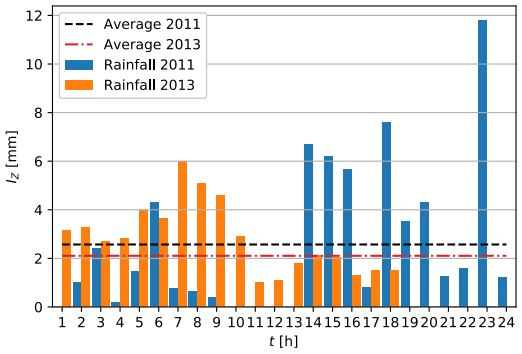

Fig. 14. Rainfall events on June 10th 2011 and May 23rd 2013 with average daily rainfall rates.

considered as irreducible because they are inherent to the model itself, on which the updating is performed.

Approximate likelihood formulation was implemented to facilitate Bayesian updating based on the observation of the rainfall event in 2011 and the corresponding initiation zones. Based on the discretized initiations zones in Fig. 13, eight separate initiation zones were detected, C_{Fi}, $i = 1, \ldots, 8$. The likelihood function for each of those zones was derived by interpreting the observation of landslide initiation as the global factor of safety within the initiation zone greater than one before the rainfall, $F_S^g(\boldsymbol{x}, t = 0) > 1$, and equal to one at the end of the rainfall, $F_S^g(\boldsymbol{x}, t = T) = 1$. Alternative likelihood formulations could have been considered if additional information on the failure of the respective initiation zones were available. The value of F_S^g for each of the initiation zones is approximated by the harmonic mean of the factors of safety of cells within the zone. Other potential likelihood formulations (e.g., arithmetic mean) were not analyzed due to considerable computational time required to perform the Bayesian updating. The likelihood function for C_{Fi}, $i = 1, \ldots, 8$ initiation zones is then defined as follows:

$$L_{Fi}^A(\boldsymbol{x}) = \phi\left(\frac{1 - \Theta(F_{Sp,q}(\boldsymbol{x}, t = T): (p, q) \in C_{Fi}) - \mu_{\epsilon_M}}{\sigma_{\epsilon_M}} \middle| \boldsymbol{X} = \boldsymbol{x}\right)$$

where p and q are the cell indexes, Θ is the harmonic mean, $\boldsymbol{x}$ is a realization of the vector of random parameters, $\boldsymbol{X}$, and ϵ_M is the model error. The observation of a stable initiation zone before the rainfall is assumed to be automatically satisfied as the value of factor of safety is non-increasing for the duration of the rainfall event, $F_S(\boldsymbol{x}, t = 0) \geqslant F_S(\boldsymbol{x}, t > 0)$.

For a subset of cells where no landslide initiation was observed during the rainfall event, $C_S \subseteq C$, the approximate likelihood function is derived by interpreting the observation event as the harmonic mean of the factor of safety in those cells being larger then one before and during the rainfall event. The likelihood function can be specified as follows:

$$L_S^A(\boldsymbol{x}) = 1 - \Phi\left(\frac{1 - \min_{t\in[0,T]} \Theta\left(F_{Sp,q}\left(\boldsymbol{x}, t\right): \left(p, q\right) \in C_S\right) - \mu_{\epsilon_M}}{\sigma_{\epsilon_M}} \middle| \boldsymbol{X} = \boldsymbol{x}\right)$$

The approximate likelihood function for all of the zones is specified as follows:

$$L_A(\boldsymbol{x}) = L_S^A(\boldsymbol{x}) \prod_{i=1}^{8} L_{Fi}^A(\boldsymbol{x})$$

6.3. Results and discussion

Fig. 15(a) and (b) present the posterior mean of $F_S(\boldsymbol{x}, t = 0)$ within the initiation zones and the stable zone, respectively, before the 2011 rainfall event. From Fig. 15(a) it can be observed that most of the cells in the initiation zone have $F_S(\boldsymbol{x}, t = 0)$ values greater than one with a smaller number of cells having values lower than one. These values are consistent with the interpretation of F_S^g as a harmonic mean of the factors of safety in the initiation zones being greater than one before the rainfall. Similar observations can be detected from Fig. 15(b) in the stable zone, with most of the cells being stable and a smaller number of cells having a factor of safety smaller than one.

Fig. 15(c) and (d) present the posterior mean of $F_S(\boldsymbol{x}, t = T)$ within the initiation zones and the stable zone, respectively. When comparing Fig. 15(a) and (c), one can observe that a greater number of cells in the initiation zones has a factor safety close to or lower than one. This agrees with the observation of F_S^g within each of the initiation zones being interpreted as a harmonic mean equal to one after the rainfall event. The comparison of Fig. 15(b) and (d) shows that the factors of safety of cells in the stable zone have lower values after the rainfall event. However, most of the cells are stable thus indicating that F_S^g in the stable zone is greater than one.

Fig. 15(e) shows the posterior mean of c in the initiation zones. From Fig. 15(e) it can be detected that the updating process resulted in reduced mean values with the posterior values in many of the cells being lower than the prior mean of 4000 Pa. Such change is consistent with the observation of landslide initiation in those zones as a decrease in the value of c contributes to destabilizing the slope. In the stable zones, the updating process has resulted in increased mean values of c in some of the areas and reduces values in other areas, as shown in Fig. 15(f). When investigating the results of the updating process and its effects on the model parameters it is important to note that the posterior values of model parameters at a given cell are not influenced only by conditions at the cell but also by the conditions at the neighboring cells (e.g., initiation zones) due to the presence of spatial correlation. One of the potential reasons for increased mean values of c in some areas of the stable zone is that an observation of a stable zone was observed on relatively steep slopes. To ensure stability on such steep areas, the value c was increased in the updating process to achieve the

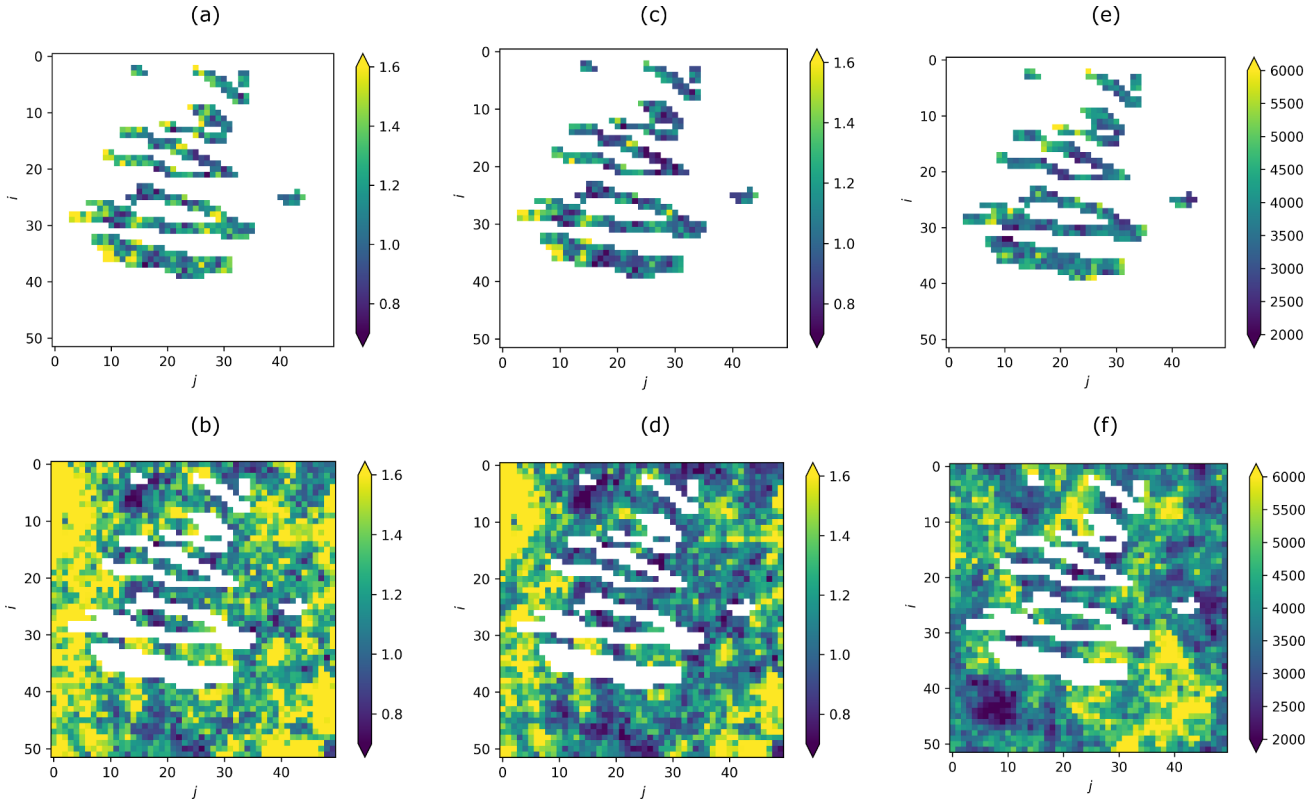

Fig. 15. (a) Posterior mean of $F_S(\boldsymbol{x}, t = 0)$ within the landslide initiation zones, (b) Posterior mean of $F_S(\boldsymbol{x}, t = 0)$ in the stable zone, (c) Posterior mean of $F_S(\boldsymbol{x}, t = T)$ within the landslide initiation zones, (d) Posterior mean of $F_S(\boldsymbol{x}, t = T)$ in the stable zone, (e) Posterior mean of c [Pa] within the landslide initiation zones, (f) Posterior mean of c [Pa] in the stable zone.

specified observation. In reality, the stability of those cells could have been also explained by parameters and conditions not captured by the model such as the effects of vegetation or slope geometry. The effects of the updating process on the distribution of F_S^g in the largest initiation zone (i.e., second from below in Fig. 15(a)) is presented in Fig. 16. Fig. 16 shows prior and posterior distributions of F_S^g after the rainfall, $t = T$. From Fig. 16 it can be observed that the updating process has significantly reduced variability in the values of F_S^g to agree with the interpretation of the landslide initiation zone as the harmonic mean of the factors of safety of the cells within the initiation zone being equal to one. These results indicate that the updating process is capable of significantly reducing uncertainties in the model parameters with the resulting variability in the posterior distribution of F_S^g providing a basis for an improved landslide hazard assessment.

Fig. 17(a) and (b) show the effects of updating on the mean values of ϕ in the initiation zones and the stable zone. From Fig. 17(a) it can be detected that the updating process resulted in the reduction of mean values of ϕ in the initiation zones with the posterior mean being lower than the prior mean of 32°. Such change is consistent with the observation of landslide initiation in those zones as a decrease in the value of ϕ contributes to destabilizing the slope. The posterior means of ϕ in the stable zone feature both increasing and decreasing values, similar to the interpretation of posterior values of c. The updating process also resulted in reduced variability in the model parameters, which indicates that the updating process provides a basis to improve the knowledge about uncertain parameters and improve assessment of landslide initiation. Other model parameters are not being presented in detail as no clear visual patters between the posterior mean and standard deviation, and the initiation and the stable zones were detected. However, this does not exclude the possibility that the other model parameters might be significantly affected by the updating process in different settings.

The effects of the updating process on the estimates of the probability of landslide initiation are presented in Fig. 17(c) and (d). Fig. 17(c) presents the estimates of the probability of landslide initiation based on prior information after the rainfall event of 2011. The initiation zones were left transparent as the landslide initiation was realized in the cells of those zones. From Fig. 17(c) it can be observed that a substantial ratio of cells in the studied domain has relatively high probabilities of landslide initiation with the highest values above 0.4.

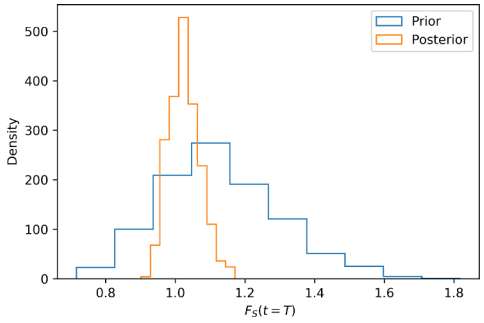

Fig. 16. Prior and posterior distribution of $F_S^g(\boldsymbol{x}, t = T)$ in the largest landslide initiation zone (i.e., second from below).

The effects of updating on the estimates of the probability of initiation can be examined in Fig. 17(d). From Fig. 17(d) it can be detected that the updating process resulted in a significant increase of probabilities of landslide initiation with the highest values being above 0.8. However, in some regions the updating process results in reduced probabilities of landslide initiation. The largest positive difference between the posterior and prior values of around 0.8 demonstrates that the updating process can result in increasing the likelihood of landslide initiation by reducing uncertainties in the knowledge on spatially variable model parameters. Increases in the likelihood of landslide initiation are associated with cells that are often in the proximity of the

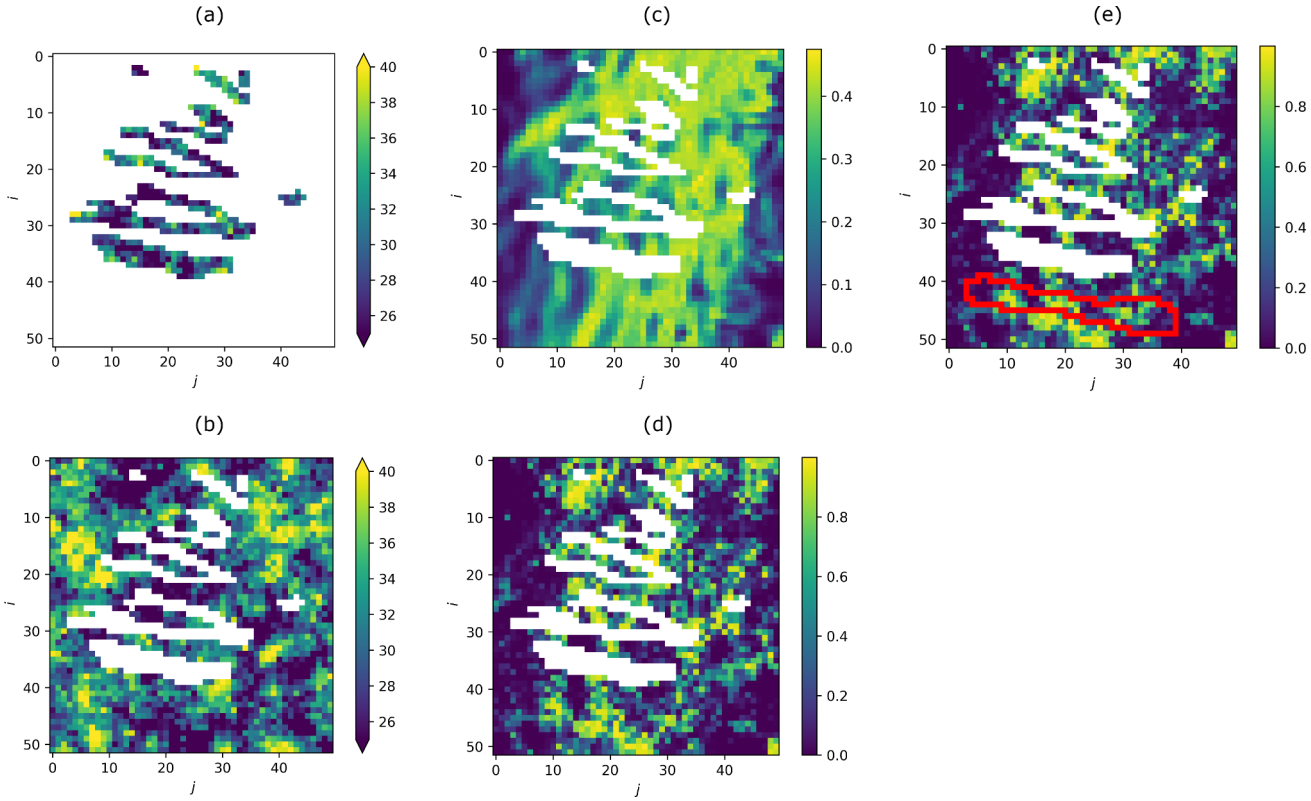

Fig. 17. (a) Posterior mean of ϕ [°] within the landslide initiation zones, (b) Posterior mean of ϕ [°] in the stable zone, (c) Prior failure probability after the rainfall event of 2011, (d) Posterior failure probability after the rainfall event of 2011, (e) Posterior failure probability with the contours of the landslide initiation zone after the rainfall event of 2013 highlighted.

landslide initiation zones where updating process resulted in reduced mean values of c and ϕ, as observed in Figs. 15(f) and 17(b). Such estimates are reasonable as decreasing values of both c and ϕ contribute to destabilizing the slope and consequently increasing the likelihood of landslide initiation.

Conversely, reduction of uncertainties in the model parameters through the implemented updating process can also result in reduced likelihood of landslide initiation. For some cells within the studied domain, the reduction was significant with the reduction of 0.4 from prior to posterior estimates of the probability of landslide initiation. Such conditions can be found in cells that had relatively high prior likelihood of landslide initiation, which is likely to be associated with cells on relatively steep sections of the model domain. Given that such areas remained stable after the rainfall event of 2011, the updating process increased the stability of such cells to achieve agreement between the observation and model predictions. Increased stability of those cells is consequently achieved through higher posterior means of stabilizing model parameters such as c and ϕ and reduced variability around those values when compared to the prior distributions. These results demonstrate the advantages of the implemented updating process to explicitly calibrate spatially variable parameters of landslide prediction models with observations of landslide initiation zones and contribute to an improved and more refined landslide hazard assessment.

The performance of the updating process and its capacity for providing an improved and more refined landslide hazard assessment were examined by simulating the rainfall event of 2013 in TRIGRS. As discussed earlier, the rainfall event of 2013 triggered multiple landslides in the Kvam area with one of the landslide initiation zones being within the study domain, as shown in Fig. 13. The landslide initiation zones corresponding to the rainfall event of 2011 remained inactive during the 2013 rainfall event and their stability was not assessed.

The stability of the cells that remained stable or were within the runout zones after the landslide event of 2011 was assessed again by simulating the rainfall event of 2013. The stability of cells in the runout zones were evaluated based on their original geometry due to lack of information on the post-landslide geometry and depths to bedrock. The stability of the cells was assessed on samples from the posterior distribution of the model parameters obtained with the updating process based on the 2011 rainfall event. Estimated probabilities of landslide initiation for the rainfall event of 2013 are presented in Fig. 17(f). The contours of the landslide initiation zone following the rainfall event of 2013 is highlighted in red in Fig. 17(f). From the estimated values within the initiation zone after the 2013 event, one can observe that there are several zones of high probability of landslide initiation with the probabilities being greater than 0.8. Instabilities in those zones could have been the initial unstable zones that triggered the propagation of the failure zone and resulted in landslide initiation. These results indicate that the provided estimates of the probabilities of landslide initiation are consistent with the observed landslide initiation zone after the 2013 rainfall event. Such estimates can contribute to improving and refining landslide hazards assessments by continuously integrating new observations and updating the model parameters.

Additionally, there are several addition zones with high probability of landslide initiation in cells that remained stable after the 2011 rainfall event. As discussed earlier, many of these zones are found in the proximity of the prior landslide initiation zones and on the runnout paths of the corresponding zones. Such high estimates of probability are affected by the conditions at those cells (e.g., relatively steep slope) but also on the nearby observations of unstable cells, which may contribute to increasing the likelihood of landslide initiation due to the effects of spatial correlation of the model parameters. Potential explanations for the stability of those cells can be multiple including inadequate assumptions or knowledge about the actual conditions (e.g., slope, surface cover, model parameters), geometry changes (e.g., changes slope profile in the runnout zones) or inadequacy of the landslide prediction

model to accurately assess the stability of those cells. However, it is important to note the updating process has reduced the size of the areas with high probabilities of landslide initiation that remained stable after the rainfall event, as seen from the comparison of Fig. 17(c) and (d).

7. Overall discussions

The implementation of physical-based models often relies on calibration with observations to improve knowledge on the uncertain model parameters due to the common lack of data on the model parameters. The calibration strategy developed in this study builds on the statistical modeling of spatially variable soil properties by adopting the Bayesian framework to update the uncertain parameters. The Bayesian updating framework is versatile and can include various types of observations with the focus of this study being calibration based on landslide inventories (e.g., observations of landslide initiation zones). The developed approach for model calibration introduced several novelties to overcome challenges related to large numbers of calibration parameters and high-dimensional likelihood functions. The former challenge arises from the explicit modeling of spatially variable model parameters with random fields. This was resolved by reformulating the Bayesian updating problem as an equivalent reliability problem with the BUS approach. The equivalent reliability problem was solved with the SUS reliability method, which is efficient in problems with large number of parameters. The latter challenge appears in Bayesian updating problems with relatively large number of cell-based observations (e.g., cells failing after a rainfall event), resulting in high-dimensional likelihood functions. Evaluating such likelihood functions is challenging because their values can become very low and computationally intractable. This challenge was resolved by developing novel approximate likelihood formulations suitable for the interpretation of observations from landslide inventories. The novel likelihood formulations are based on the ABC method, where a lower-dimensional likelihood function is formulated based on certain summary statistics to avoid computational difficulties of the higher-dimensional full likelihoods. Different types of approximate likelihood formulations, specific for physical-based landslide prediction models, were implemented and their performance was examined on several examples.

The effects of updating within the initiation zone also expand to the neighboring zones that remained stable after the rainfall event due to the explicit modeling of spatial dependence of model parameters as modeled by the autocovariance function of the random field model. The observation of the landslide initiation zone was associated with lower mean and reduced standard deviation values of soil strength parameters, such as cohesion and friction angle. These results are considered as reasonable as lower values of strength parameters decrease the capacity of a slope to remain stable, thus satisfying the observation of landslide initiation. Conversely, higher mean values of diffusivity were associated with the observation of a landslide initiation zone as higher diffusivity values contribute to faster rainfall infiltration into the slope and consequently more rapid destabilization of the slope. These changes are less pronounced as the distance from the initiation zone increases with the mean values of strength parameters in the stable zones being equal or slightly higher than the ones assumed before calibration. This agrees with the effects of increasing strength parameters on stabilizing the slope.

In addition to changes in the mean values, the updating process resulted in the reduction of standard deviations of the uncertain parameters. Reducing standard deviation increases knowledge on uncertain model parameters and enables a more refined assessment of landslide hazards. The reduction in the standard deviation was strongest in the initiation zones and in the stable zones in their proximity. This was a consequence of the landslide initiation zone providing a stronger updating information in the considered example and being more restrictive on the range of likely parameters values based on the knowledge prior to updating. Improving knowledge on the uncertain model parameters has important effects on the landslide hazard assessment. These effects were quantified by calculating the probability of landslide initiation in the zones that remained stable after the rainfall event. The updated knowledge lead to increased probabilities of landslide initiation in the cells in the proximity of the observed landslide initiation zones. This is due to the effects of spatial dependence on propagating the reduction in strength parameters from the landslide initiation zones to the neighboring stable areas. Conversely, a decrease in the probability of landslide initiation was observed in some cells that remained stable after the rainfall event. The decrease in probability of landslide initiation in those areas is explained by these cells usually being found on steep slopes with higher values of strength parameters being required to stabilize them. These results indicate that the implemented updating strategy contributes to a more refined and improved landslide hazard assessment.

In addition to the potential of the developed approach to improve landslide hazard assessment, it is important to highlight several limitations of the implemented approach. One of the limitations is that the calibration is model-based with the formulation of the likelihood functions and the results of the updating being dependent on the implemented physical-based model. The approximate likelihood formulations are developed on approximations of F_S^g based on the values of factor of safety in the cells of the initiation zone. Such approach is suited to typical physical-based landslide prediction models and it does not account for the equilibrium of forces between the cells and the nonlinear redistribution forces in the landslide propagation process. These approximations could be avoided by implementing more advanced models that can account explicitly for the limitations of these models. Furthermore, the interpretation of the updating results is dependent on the formulations of physical processes included in the model and its capacity to realistically simulate the landslide initiation process. The interpretation of the results should be done within the context of the implemented model as the updating process will aim to update the distributions of the model parameters to achieve parity between the observations and the model predictions. Given that the parity is based only on the functionality embedded in the implemented landslide model, it is important to avoid applying a model that does not contain features observed in reality. The assumption that the implemented model is capable to realistically simulate the conditions observed in reality together with its limitations should be thoroughly examined. In case that the model is considered suitable, the implemented approach quantifies the effects of model uncertainty with a model error term. However, it is important to note that the model error applies for the situations when the model is considered to be able to realistically simulate the observed conditions. In addition to ensuring that the applied model is suitable, the application of more advanced models that feature, among other, explicit modeling of the landslide initiation process and post-failure behavior, soil anisotropy, three-dimensional groundwater flow, and surface flow modeling could contribute to an improved landslide hazard assessment with the developed framework. Additional limitation is that the implemented Bayesian framework is computationally intensive with the computational demands increasing with the size of the domain and required accuracy in the posterior parameter values. Analyses with larger numbers of cells may benefit from further improvement in efficiency of Bayesian updating algorithms or require higher computational resources and parallel computing.

8. Conclusions

This study presented a novel framework for Bayesian calibration of spatially distributed physical-based landslide prediction models. The study introduced several novelties including modeling of spatially variable model parameters with random fields and new approximate likelihood formulations to support efficient calibration of such models with observations from landslide inventories.

The study demonstrated that the developed approach is capable of successfully updating the model parameters and overcoming the challenges of large numbers of parameters and high-dimensional likelihood functions characteristic for such calibration problems. Enabled by the

approximate likelihood formulation, an efficient relation between the observation of a landslide initiation zone and the corresponding model prediction was established to facilitate updating of model parameters. The developed Bayesian calibration strategy significantly affected the distribution of model parameters within the landslide initiation zones. These results indicate that the implemented strategy contributes to a more refined and improved landslide hazard assessment.

CRediT authorship contribution statement

Ivan Depina: Conceptualization, Data curation, Formal analysis, Funding acquisition, Investigation, Methodology, Project administration, Resources, Software, Supervision, Validation, Visualization, Writing - original draft, Writing - review & editing. **Emir Ahmet Oguz:** Conceptualization, Data curation, Formal analysis, Methodology, Validation, Writing - review & editing. **Vikas Thakur:** Conceptualization, Formal analysis, Funding acquisition, Investigation, Methodology, Resources, Supervision, Validation, Writing - review & editing.

Declaration of Competing Interest

The authors declare that they have no known competing financial interests or personal relationships that could have appeared to influence the work reported in this paper.

Acknowledgments

The authors acknowledge the support from the Research Council of Norway and several partners through the research projects KlimaDigital and Klima2050. The authors also acknowledge the support of the Croatian Science Foundation through the innovation project INFRA.

Appendix A. Transient pressure head component

The transient component of the groundwater pressure head for tension saturated initial conditions with a time-varying flux at the ground surface and a zero flux at impermeable basal boundary at a finite depth (Baum et al., 2002) is calculated as follows:

$$\psi_t\left(z,\, t\right) = 2\sum_{n=1}^{N}\frac{I_{nZ}}{k_S}H_f\left(t-t_n\right)[D_1(t-t_n)]^{1/2}\cdot$$
$$\sum_{b=1}^{\infty}\left\{\text{ierfc}\left[\frac{(2b-1)H-(H-z)}{2[D_1(t-t_n)]^{1/2}}\right]+\text{ierfc}\left[\frac{(2b-1)H+(H-z)}{2[D_1(t-t_n)]^{1/2}}\right]\right\}$$
$$-2\sum_{n=1}^{N}\frac{I_{nZ}}{k_S}H_f\left(t-t_{n+1}\right)[D_1(t-t_{n+1})]^{1/2}\cdot$$
$$\sum_{b=1}^{\infty}\left\{\text{ierfc}\left[\frac{(2b-1)H-(H-z)}{2[D_1(t-t_{n+1})]^{1/2}}\right]+\text{ierfc}\left[\frac{(2b-1)H+(H-z)}{2[D_1(t-t_{n+1})]^{1/2}}\right]\right\} \quad (37)$$

where H is depth to bedrock, I_{nZ} is the surface flux for the n^{th} time interval, N is the total number of intervals, $D_1 = D_0/\cos^2\delta$ is the relative saturated hydraulic diffusivity, $H_f(t-t_n)$ is the Heaviside step function, b is the number of the infinite series terms, and ierfc is the complementary error function.

Appendix B. Bayesian updating of a simple TRIGRS model

B.1. Problem formulation

A relatively simple Bayesian updating problem is implemented to examine updating of uncertainties associated with a simplified spatially distributed landslide prediction model and the geometry presented in Fig. 2. The stability is evaluated, for each of the cells, with TRIGRS based on the value of F_S as defined in Eq. (4). The set of uncertain model parameters is defined as $\boldsymbol{X} = [H,\, c,\, \phi,\, H_w,\, k_s,\, D_0]^T$. The TRIGRS model parameters not included in $\boldsymbol{X}$ are considered as deterministic with the following values adopted for slope angle, $\delta = 25°$, specific dry gravity of soil, $G_s = 2.7$, void ratio, $e = 0.26$, saturated $\theta_s = 0.4$ and residual $\theta_r = 0.05$ volumetric water contents. The properties of the random model parameters and the model error, ϵ_M, are specified in Table 1.

Stability of each of the cells in the model is evaluated based on the value of F_S, such that a cell (i, j) is stable if $F_{Si,j} > 1$ and unstable if $F_{Si,j} \leqslant 1$. Based on the problem formulation, a reliability problem can be defined to estimate the probability of landslide initiation for each of the cells. For a cell (i, j), the reliability problem is defined with the performance function $g_{i,j}(\boldsymbol{X},\, \epsilon_M,\, t) = F_{Si,j}(\boldsymbol{X},\, t) + \epsilon_M - 1$. The probability of landslide initiation in a cell (i, j) after the rainfall event at time $t = T$ is calculated as $P_{Fi,j} = P(g_{i,j}(\boldsymbol{X},\, \epsilon_M,\, T) \leqslant 0)$.

B.2. Prior

Details on modeling spatial variability of the random TRIGSR parameters c, ϕ, k_s, D_0, H, and H_w are provided in Section 6.1. Meteorological observation are based on the Kvam case study and consists of a rainfall event on June 10th 2011, as presented in Section 6. The average rainfall intensity for the rainfall event in 2011 is $\bar{I}_{Z,2011} = 2.572$ [mm/h] $= 61.72$ [mm/day]. To simplify the implementation of the TRIGRS model in this example, the average rainfall intensity will be simulated over the studied 24-h period instead of the measured values.

B.3. Likelihood function

The likelihood function is formulated based on an observation of a landslide initiation zone for the given rainfall event, as shown in Fig. 2. The likelihood function will be derived from the approximate likelihood formulations in Section 4.2.3 with the likelihood formulation based on Eq. (23) for the initiation zone and the formulation in Eq. (25) for the stable zone with the harmonic means, Θ.

B.4. Posterior

Given the prior knowledge and the likelihood functions, the BUS algorithm was implemented to obtain $K = 10^4$ from the posterior distribution. Samples from the posterior distributions were also used to update the reliability estimates and evaluate the effects of the observations on the slope stability assessment. The results of the updating process are presented in Figs. B.18,B.19,B.20. Fig. B.18(a) and (c) present the posterior mean values of the factor of safety in each of the cells before and after the rainfall event, $F_S(\boldsymbol{x}, t = 0)$ and $F_S(\boldsymbol{x}, t = T)$, respectively. From Fig. B.18(a) it can be detected that the posterior mean values of $F_S(\boldsymbol{x}, t = 0)$ are larger than one in the entire domain, corresponding to the observation that F_S^g in the initiation and the stable zones are greater then one. From Fig. B.18(c) it can be observed that the posterior mean values within the cells of the initiation zone are close to or lower than one, corresponding to the observation that F_S^g in the initiation zone is lower or equal to one. The posterior mean values of $F_S(\boldsymbol{x}, t = 0)$ and $F_S(\boldsymbol{x}, t = T)$ in the cells of the stable zone increase as the distance from the initiation zone increases. This is a consequence of the spatial dependence in the TRIGRS model parameters, as specified by the random field models. Additionally, from the comparison of Fig. B.18(a) and (c) it can be seen that the values of factor decrease from $F_S(\boldsymbol{x}, t = 0)$ to $F_S(\boldsymbol{x}, t = T)$ as the rainfall infiltration contributes to decreasing the slope stability. Due to relatively low number of samples there is lack of symmetry (i.e., vertical and horizontal with respect to the initiation zone) in the estimated statistics.

Fig. B.18(b) and (d) present the values of posterior standard deviation of $F_S(\boldsymbol{x}, t = 0)$ and $F_S(\boldsymbol{x}, t = T)$, respectively. From Fig. B.18(b) and (d) it can be detected that the updating process leads to lowered values of standard deviation with the greatest reduction found within the initiation zone. This can be explained by the observation of landslide initiation providing stronger updating information and being more restrictive to the range of possible outcomes as specified by the prior knowledge. Within the stable zone, the reduction of standard deviation values is stronger in the proximity of the initiation zone due to the effects of spatial dependence in the TRIGRS model parameters.

Given that the approximate likelihood function is specified in terms of F_S^g, the updating process will be examined in terms of the values of F_S^g to satisfy the observation of landslide initiation. Fig. B.18(e) and (f) present, respectively, the histograms of the prior and posterior samples of $F_S^g(\boldsymbol{x}, t = 0)$ and $F_S^g(\boldsymbol{x}, t = T)$ in the initiation zone. Fig. B.18(e) reveals that the updating process significantly reduces variability in the values of $F_S^g(\boldsymbol{x}, t = 0)$ based on the observation of a stable slope before the rainfall event and landslide initiation after the rainfall event. The capacity of the implemented framework to satisfy those observations can be evaluated from the posterior histograms. The posterior histogram of $F_S^g(\boldsymbol{x}, t = 0)$ in Fig. B.18(e) shows that most of the samples are above one and satisfy the observation of a stable slope before the rainfall event with some realizations being below one due to the effects of the model error. After the rainfall event, the distribution of $F_S^g(\boldsymbol{x}, t = T)$ shifts to the left, as seen from Fig. B.18(f), with the majority of samples being lower than one and agreeing with the observation of landslide initiation. However, a significant ratio of samples is above one due to the effects of the model error on the updating process. The results in Fig. B.18(e) and (f) demonstrate that the results of the implemented updating process are consistent with the interpretations of the landslide initiation process as $F_S^g(\boldsymbol{x}, t = 0) > 1$ and $F_S^g(\boldsymbol{x}, t = T) \leqslant 1$, and corresponding approximate likelihood formulation. These results indicate that the implemented approximate likelihood formulation and the updating process can support updating process based on observations of landslide initiation zones.

The effects of updating on the distributions of the TRIGRS model parameters can be examined in Figs. B.19 and B.20. The focus will be on c, ϕ and D_0 as no noticeable effects of the updating process on the distributions of the other parameters could be detected. Fig. B.19(a) and (b) show, respectively, the posterior mean and standard deviation of c in Pa. From Fig. B.19(a) one can detect that the initiation process is likely to be

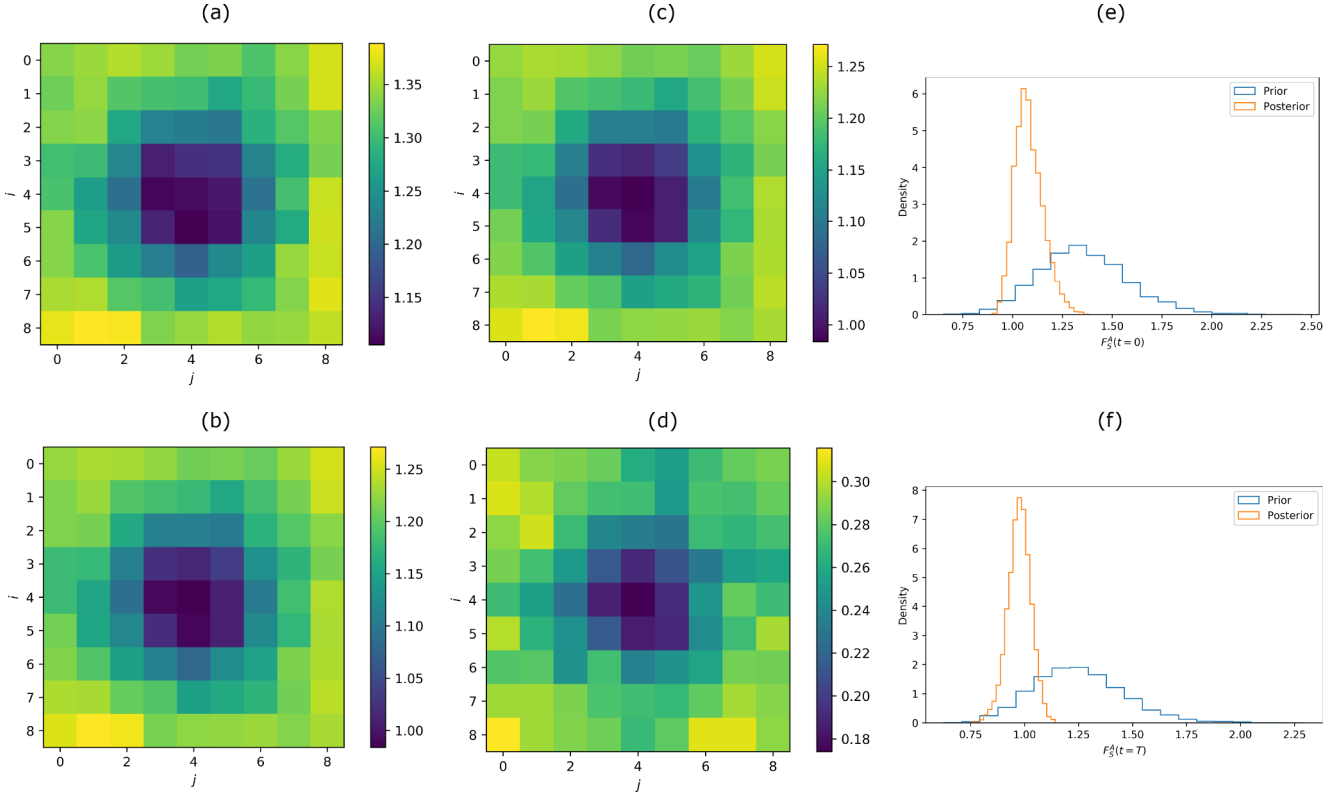

Fig. B.18. (a) Posterior mean of $F_S(\boldsymbol{x}, t = 0)$, (b) Posterior standard deviation of $F_S(\boldsymbol{x}, t = 0)$, (c) Posterior mean of $F_S(\boldsymbol{x}, t = T)$, (d) Posterior standard deviation of $F_S(\boldsymbol{x}, t = T)$, (e) Prior and posterior distributions of $F_S^g(\boldsymbol{x}, t = 0)$ in the initiation zone, (f) Prior and posterior distributions of $F_S^g(\boldsymbol{x}, t = T)$ in the initiation zone.

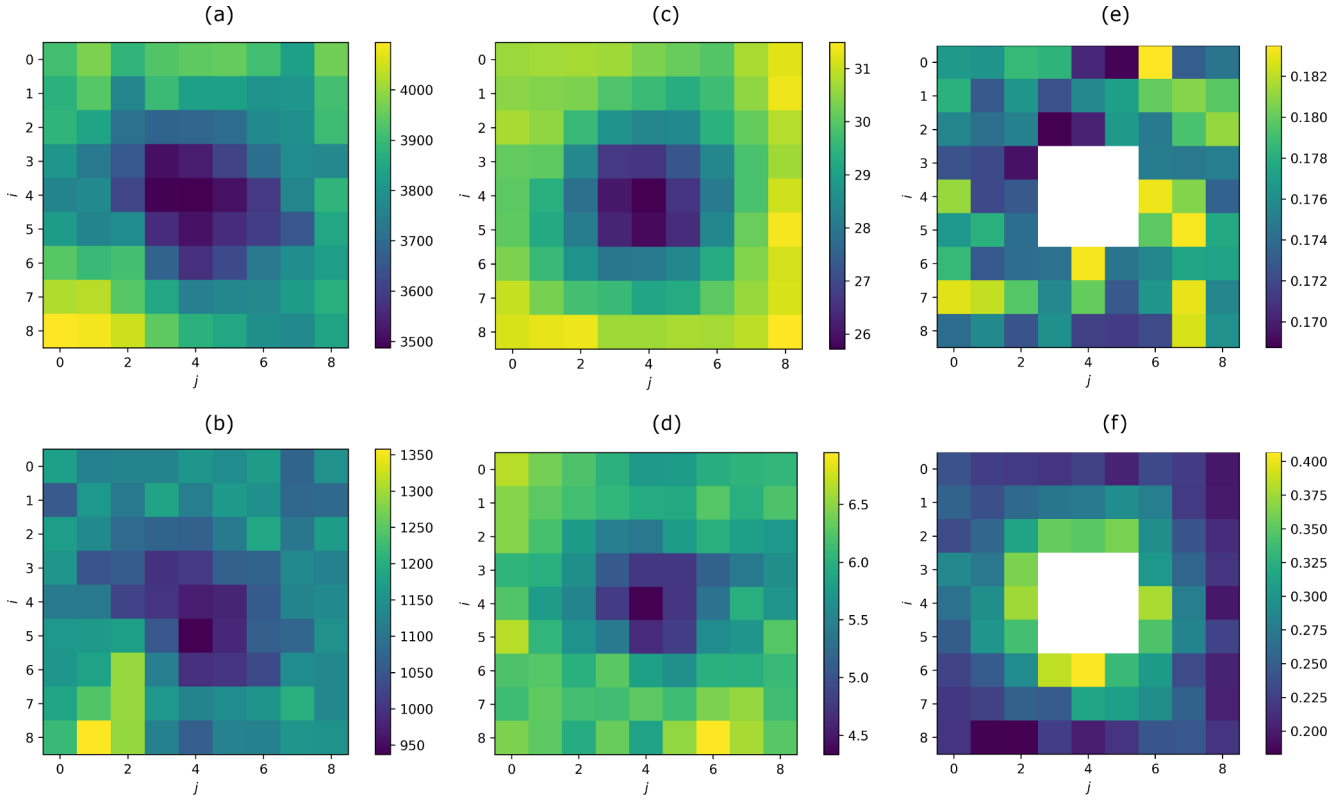

Fig. B.19. (a) Posterior mean of c [Pa], (b) Posterior standard deviation of c [Pa], (c) Posterior mean of ϕ [°], (d) Posterior standard deviation of ϕ [°], (e) Prior failure probability, P_F, (f) Posterior failure probability, P_F''.

associated with lower values of c when compared to the prior mean of 4000 Pa with the lowest values being around 3500 Pa. This is reasonable as lower values c decrease the soil strength and the capacity of slopes to remain stable thus contributing to satisfying the observation of landslide initiation. Within the stable zone, the posterior mean values of c increase with the distance from the initiation zone to the values equal or slightly higher than the prior mean values. The gradual increase with the distance from the initiation zone is attributed to the spatial dependence of c modeled by the lognormal random field. Higher mean values in some cells can be attributed to the observation of a cell being stable after the rainfall event being associated to higher soil strength parameters or the effects of the iterative sampling process and the limited number of samples. Fig. B.19(b) shows the effects of the updating process on the posterior standard deviation of c. In general, the updating process results in reduced values

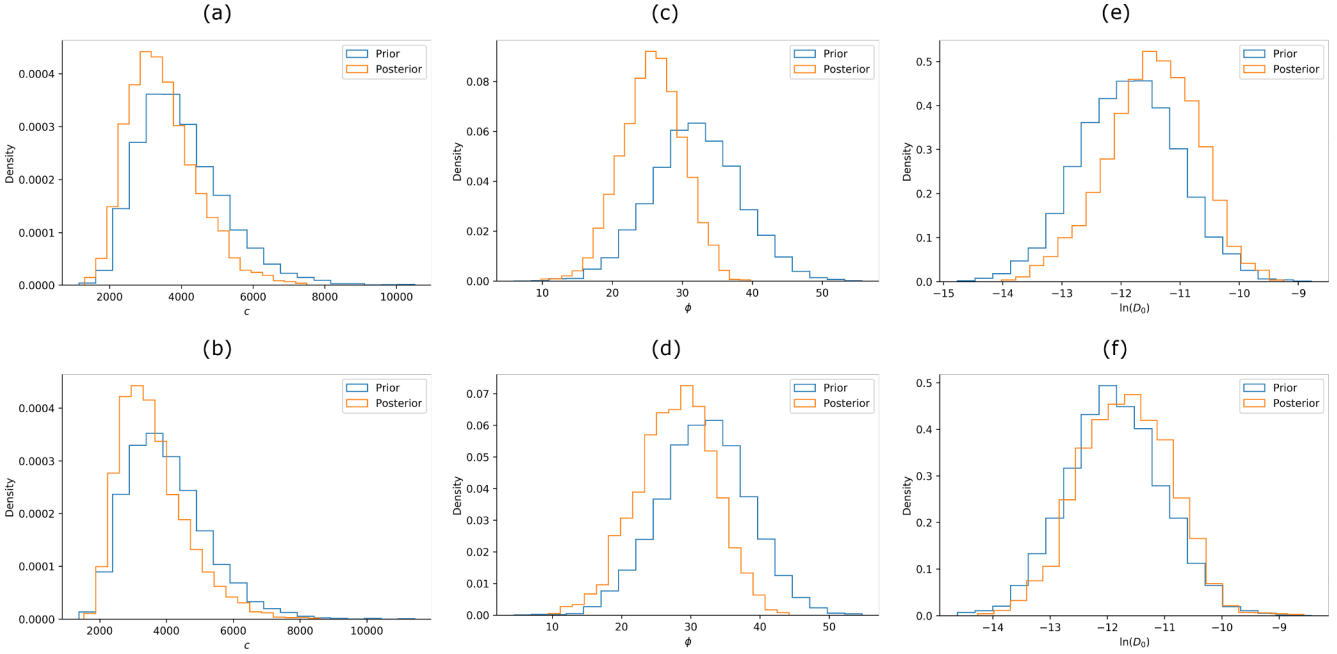

Fig. B.20. Prior and posterior distributions of: (a) c [Pa] at cell (4, 4), (b) c [Pa] at cell (2, 4), (c) ϕ [°] at cell (4, 4), (d) ϕ [°] at cell (2, 4), (e) $\ln(D_0)$ at cell (4, 4), (f) $\ln(D_0)$ at cell (2, 4).

of standard deviation from the prior value of 1200 Pa with the greatest decrease being in the initiation zone. This contributes to increasing knowledge about the uncertain model parameters for a better landslide hazard assessment. However, in some cells of the model increased values of standard deviation are observed. This likely to be associated with the effects of the iterative sampling process and the limited number of samples.

Fig. B.19(c) and (d) provide an insight in the effects of the updating process on the posterior mean and standard deviation of ϕ. Fig. B.19(c) reveals that the updating process leads to reduced posterior mean values of ϕ when compared to the prior mean of 32°. Largest reduction is observed within the initiation zone with the mean values increasing with distance from the initiation zone to the values close to the prior ones at the edges of the model domain. These trends seem reasonable as lower values of soil strength parameters as ϕ reduce the capacity of slopes to remain stable during a rainfall event thus contributing to satisfying the observation of landslide initiation. The gradual trend of increasing posterior mean values with the distance from the initiation zone is attributed to the spatial dependence of ϕ modeled by the normal random field. Fig. B.19(d) presents the posterior values of the standard deviation of ϕ. The updating process resulted in decreased values of standard deviation in most of the cells with some exceptions. These exceptions are likely to be associated with the effects of the iterative sampling process and the limited number of samples. Similar as for the values of c, the greatest reduction is observed within the cells of the initiation zone. Reducing variability in the model parameters contributes to increasing knowledge about the uncertain model parameters for a better landslide hazard assessment.

The effects of updating on the estimates of the probability of landslide initiation in the cells of the stable zone are examined in Fig. B.19(e) and (f). Fig. B.19(e) presents the prior estimates of the probability of landslide initiation after the rainfall event. The probability estimates in Fig. B.19(e) are based on the prior distributions of model parameters. The initiation zones were left transparent as the landslide initiation was realized in the cells of those zones. From Fig. B.19(e) it can be observed that the probability of landslide initiation vary in the range between 0.168 and 0.184. The observed variability is due to relatively small number of samples used to obtain those estimates.

The effects of updating on the estimates of the probability of initiation can be examined in Fig. B.19(f). Fig. B.19(f) presents the posterior estimates of the probability of landslide initiation after the rainfall event. From Fig. B.19(f) it can be detected that the updating process resulted in a significant increase of probabilities of landslide initiation with the highest values being above 0.4. The largest increase between the posterior and prior values is observed in the proximity of the initiation zone and it demonstrates that the updating process can result in increasing the likelihood of landslide initiation by reducing uncertainties in the knowledge on spatially variable model parameters. Increases in the likelihood of landslide initiation are associated with cells that are often in the proximity of the landslide initiation zones where updating process resulted in reduced mean values of c and ϕ, as observed in Fig. B.20(b) and (d). Such estimates are reasonable as decreasing values of both c and ϕ contribute to destabilizing the slope and consequently increasing the likelihood of landslide initiation.

The updating process can be further examined by investigating the prior and posterior distributions of TRIGRS model parameters at selected cells in the model. Fig. B.20(a) shows histograms of prior and posterior samples of c from a cell in the initiation zone. Similarly, Fig. B.20(b) presents histograms of prior and posterior samples of c from a cell in the stable zone and on the edge of the initiation zone. From Fig. B.20(a) it can be seen that the updating produced a distribution with the mean shifted to the left and reduced variance. The shape of the posterior distribution is relatively similar to the prior lognormal distribution. As discussed earlier, this is consistent with the observation of landslide initiation at this cell. Similar observations can be made for the histogram in Fig. B.20(b). However, in this case an increase in the mean would be expected due to the cell remaining stable after the rainfall event. Conversely, a decrease in the mean was observed due to spatial dependence of c as modeled by the lognormal random field.

Fig. B.20(c) presents histograms of prior and posterior samples of ϕ from a cell in the initiation zone. Similarly, Fig. B.20(d) shows histograms of prior and posterior samples of ϕ from a cell in the stable zone on the edge of the initiation zone. Fig. B.20(c) demonstrates that the updating produced a distribution with the mean shifted to the left and reduced variance. These trends are consistent with the observation of landslide initiation at this cell, as discussed earlier. Similar trends are observed in the posterior histogram in Fig. B.20(d) with the decrease in the mean being less distinct. Fig. B.20(e) presents the effects of the updating process on the samples of $\ln(D_0)$ from a cell in the initiation zone. Similarly, Fig. B.20(e) shows histograms of prior and posterior samples of $\ln(D_0)$ from a cell in the stable zone and on the edge of the initiation zone. Fig. B.20(e) shows that the updating produced a distribution with the mean shifted to the right. These trends are consistent with the observation of landslide initiation at this cell as higher diffusivity is associated with faster rainfall infiltration and therefore contributes to a more rapid destabilization of a slope. Similar trends are detected in the posterior histogram in Fig. B.20(e) with a smaller increase in the mean. This is likely to be attribute to the effects of spatial dependence of D_0 as modeled by the lognormal random field.

References

Au, S.-K., Beck, J.L., 2001. Estimation of small failure probabilities in high dimensions by subset simulation. Prob. Eng. Mech. 16 (4), 263–277.

Baum, R.L., Savage, W.Z., Godt, J.W., et al., 2002. TRIGRS – a fortran program for transient rainfall infiltration and grid-based regional slope-stability analysis. US Geological Survey Open-File Report 424, 38.

Cai, J.-S., Yeh, T.-C.J., Yan, E.-C., Hao, Y.-H., Huang, S.-Y., Wen, J.-C., 2017. Uncertainty of rainfall-induced landslides considering spatial variability of parameters. Comput. Geotech. 87, 149–162.

Calvello, M., Cuomo, S., Ghasemi, P., 2017. The role of observations in the inverse analysis of landslide propagation. Comput. Geotech. 92, 11–21.

Canli, E., Mergili, M., Thiebes, B., Glade, T., 2018. Probabilistic landslide ensemble prediction systems: lessons to be learned from hydrology. Nat. Hazards Earth Syst. Sci. 18, (8).

Chen, H.X., Zhang, L.M., 2014. A physically-based distributed cell model for predicting regional rainfall-induced shallow slope failures. Eng. Geol. 176, 79–92.

Dai, F., Lee, C., Ngai, Y.Y., 2002. Landslide risk assessment and management: an overview. Eng. Geol. 64 (1), 65–87.

Depina, I., Wolebo, A.P., 2017. Application of conditional random fields for the reliability assessment of slope stability. In: 12th International Conference on Structural Safety & Reliability.

Duncan, J., Wright, S., 1980. The accuracy of equilibrium methods of slope stability analysis. Eng. Geol. 16 (1–2), 5–17.

Edvardsen, D.H., 2013. Utløsningsårsaker og utløsningsmekansimer til flomskred i moreneavsetninger.: Feltstudie av terrengtyper og inngrep i naturen som potensielt kan føre til skred inn mot fremtidige vegprosjekter. Eksempel fra Kvam, Norge. (Master's thesis). Institutt for geologi og bergteknikk, NTNU.

Fenton, G.A., Griffiths, V.D., 2008. Risk Assessment in Geotechnical Engineering. John Wiley & Sons.

Gariano, S.L., Guzzetti, F., 2016. Landslides in a changing climate. Earth Sci. Rev. 162, 227–252.

Holm, G., 2012. Case study of rainfall induced debris flows in Veikledalen, Norway, 10th of June 2011, University of Oslo, Master's thesis.

Iverson, R.M., 2000. Landslide triggering by rain infiltration. Water Resour. Res. 36 (7), 1897–1910.

Janbu, N., et al., 1989. Grunnlag i geoteknikk, Tapir.

Khalaj, S., BahooToroody, F., Abaei, M.M., BahooToroody, A., De Carlo, F., Abbassi, R., 2020. A methodology for uncertainty analysis of landslides triggered by an earthquake. Comput. Geotech. 117, 103262.

Kim, S., Fiedler, B.J., Kim, S., 2018. A landslide model with the shear band propagation: modification for unsaturated condition. IFCEE 314–323.

Lacasse, S., Nadim, F., 1996. Uncertainties in characterising soil properties. In: Uncertainty in the geologic environment: From theory to practice, ASCE. pp. 49–75.

Liu, K., Vardon, P., Hicks, M., 2018. Sequential reduction of slope stability uncertainty based on temporal hydraulic measurements via the ensemble kalman filter. Comput. Geotech. 95, 147–161.

Melchiorre, C., Frattini, P., 2012. Modelling probability of rainfall-induced shallow landslides in a changing climate, Otta, Central Norway. Clim. Change 113 (2),

413–436.
Mergili, M., Marchesini, I., Rossi, M., Guzzetti, F., Fellin, W., 2014. Spatially distributed three-dimensional slope stability modelling in a raster gis. Geomorphology 206, 178–195.
Montgomery, D.R., Dietrich, W.E., 1994. A physically based model for the topographic control on shallow landsliding. Water Resour. Res. 30 (4), 1153–1171.
Montrasio, L., Valentino, R., 2008. A model for triggering mechanisms of shallow landslides. Nat. Hazards Earth Syst. Sci. 8 (5), 1149–1159.
NGU, Geological Survey of Norway (2019).https://www.ngu.no/.
Pack, R.T., Tarboton, D.G., Goodwin, C.N., 1998. The sinmap approach to terrain stability mapping. In: 8th congress of the international association of engineering geology, Vancouver, British Columbia, Canada, vol. 21. pp. 25.
Papaioannou, I., Straub, D., 2012. Reliability updating in geotechnical engineering including spatial variability of soil. Comput. Geotech. 42, 44–51.
Pecoraro, G., Calvello, M., Piciullo, L., 2018. Monitoring strategies for local landslide early warning systems. Landslides 1–19.
Petley, D., 2012. Global patterns of loss of life from landslides. Geology 40 (10), 927–930.
Phoon, K.-K., Kulhawy, F.H., 1999. Characterization of geotechnical variability. Can. Geotech. J. 36 (4), 612–624.
Salciarini, D., Godt, J.W., Savage, W.Z., Conversini, P., Baum, R.L., Michael, J.A., 2006. Modeling regional initiation of rainfall-induced shallow landslides in the eastern Umbria Region of central Italy. Landslides 3 (3), 181.
Santoso, A.M., Phoon, K.-K., Quek, S.-T., 2011. Effects of soil spatial variability on rainfall-induced landslides. Comput. Struct. 89 (11–12), 893–900.
Schilirò, L., Montrasio, L., Mugnozza, G.S., 2016. Prediction of shallow landslide occurrence: validation of a physically-based approach through a real case study. Sci. Total Environ. 569, 134–144.
Schuëller, G., Pradlwarter, H., Koutsourelakis, P.-S., 2004. A critical appraisal of reliability estimation procedures for high dimensions. Prob. Eng. Mech. 19 (4), 463–474.
Simoni, S., Zanotti, F., Bertoldi, G., Rigon, R., 2008. Modelling the probability of occurrence of shallow landslides and channelized debris flows using geotop-fs. Hydrol. Processes: Int. J. 22 (4), 532–545.
Sisson, S.A., Fan, Y., Beaumont, M., 2018. Handbook of Approximate Bayesian Computation. Chapman and Hall/CRC.
Straub, D., 2011. Reliability updating with equality information. Probab. Eng. Mech. 26 (2), 254–258.
Straub, D., Papaioannou, I., 2014. Bayesian updating with structural reliability methods. J. Eng. Mech. 141 (3), 04014134.
The SciPy community, numpy.finfo (2019).https://docs.scipy.org/doc/numpy/reference/generated/numpy.finfo.html.
Varnes, D.J., 1958. Landslide types and processes. Landslides Eng. Practice 29 (3), 20–45.
Wang, H., Xiao, T., Li, X., Zhang, L., Zhang, L., 2019. A novel physically-based model for updating landslide susceptibility. Eng. Geol. 251, 71–80.
Yang, H.-Q., Zhang, L., Li, D.-Q., 2018. Efficient method for probabilistic estimation of spatially varied hydraulic properties in a soil slope based on field responses: a bayesian approach. Comput. Geotech. 102, 262–272.
Zhang, J., Tang, W.H., Zhang, L., 2009. Efficient probabilistic back-analysis of slope stability model parameters. J. Geotech. Geoenviron. Eng. 136 (1), 99–109.
Zhang, L., Zhang, J., Zhang, L., Tang, W., 2010. Back analysis of slope failure with Markov chain Monte Carlo simulation. Comput. Geotech. 37 (7–8), 905–912.
Zieher, T., Rutzinger, M., Schneider-Muntau, B., Perzl, F., Leidinger, D., Formayer, H., Geitner, C., 2017. Sensitivity analysis and calibration of a dynamic physically based slope stability model. Nat. Hazards Earth Syst. Sci. 17 (6), 971.
Zizioli, D., Meisina, C., Valentino, R., Montrasio, L., 2013. Comparison between different approaches to modeling shallow landslide susceptibility: a case history in Oltrepo Pavese, Northern Italy. Nat. Hazards Earth Syst. Sci. 13 (3), 559.